Noise-Driven Communication for Next-Generation Wireless Networks and IoT Systems

by

ERKİN YAPICI

A Dissertation Submitted to the
Graduate School of Sciences and Engineering
in Partial Fulfillment of the Requirements for
the Degree of

Master of Science

in

Electrical and Electronics Engineering

KOÇ ÜNİVERSİTESİ

7 July, 2025

Noise-Driven Communication for Next-Generation Wireless Networks and IoT Systems

Koç University
Graduate School of Sciences and Engineering
This is to certify that I have examined this copy of a master's thesis by

ERKİN YAPICI

and have found that it is complete and satisfactory in all respects,
and that any and all revisions required by the final
examining committee have been made.

Committee Members:

Prof. Dr. Ertuğrul Başar (Advisor)

Asst. Prof. Murat Kuşçu

Prof. Dr. Ali Emre Pusane

Date:

I dedicate this thesis to Mehmet Fikri Yapıcı, whose memory and legacy continue to inspire me.

ABSTRACT

Noise-Driven Communication for Next-Generation Wireless Networks and IoT Systems
ERKİN YAPICI
Master of Science in Electrical and Electronics Engineering
7 July, 2025

Current advancements in the wireless communications have opened new opportunities for low-data-rate Internet-of-Things (IoT) systems. Legacy communication frameworks which rely on high-complexity operations on signal processing and strict synchronization requirements, often fail to meet the low bit error rate (BER), energy harvesting capability, and ability to operate reliably at low data rates, key requirements of modern and future IoT networks. To address these limitations, noise-domain modulation techniques have emerged, encoding data not into the deterministic parameters like frequency or phase, but into the statistical properties such as mean, variance and the correlation of the artificially generated Gaussian noise. These schemes eliminate the need for power allocation and also the successive interference cancellation (SIC), which reduces the complexity and energy consumption. To clarify, by eliminating the need for synchronization and equalization, these techniques enable suitable communication for dynamic and unpredictable wireless environments.

Chapter 3, presents an innovative joint energy harvesting (EH) and communication scheme for IoT devices by leveraging the emerging noise modulation (NoiseMod) technique. The proposed approach embeds information into the mean value of real Gaussian noise samples to enable wireless energy and information harvesting. We propose a mean-based detector to decode the information and derive the analytical bit error probability (BEP) of the proposed scheme under Rician fading channels. We utilize a nonlinear rectenna model to demonstrate the feasibility of the proposed scheme in terms of energy harvesting capability. Simulation results demonstrate that the proposed method outperforms conventional modulation techniques in terms of EH performance across various channel conditions while maintaining reliable communication performance for next-generation IoT networks.

In Chapter 4, noise-domain non-orthogonal multiple access (ND-NOMA), an innovative communication scheme that utilizes the modulation of artificial noise mean and variance to convey information, is presented. Distinct from traditional methods such as power-domain non-orthogonal multiple access (PD-NOMA) that heavily rely on SIC, ND-NOMA utilizes the noise domain, considerably reducing power consumption and system complexity. Inspired by noise modulation, ND-NOMA enhances energy efficiency and provides lower BEP, making it highly suitable for next-generation IoT networks. Our theoretical analyses and computer simulations reveal that ND-NOMA can achieve exceptionally low bit error rates in both uplink and downlink scenarios, in the presence of Rician fading channels. The proposed multi-user system is supported by a minimum distance detector for mean detection and a threshold-based detector for variance detection, ensuring robust communication in low-power environments. By leveraging the inherent properties of noise, ND-NOMA offers a promising platform for long-term deployments of low-cost and low-complexity devices.

Ultimately, in the Chapter 5, a novel three-user noise-domain non-orthogonal multiple access ND-NOMA scheme by introducing the correlation as a new dimension besides mean and variance quantities used in two-user ND-NOMA is proposed. The new three-user ND-NOMA scheme includes both uplink and downlink scenarios, with detectors designed to decode the information embedded in mean, variance, and correlation. Our theoretical analysis and simulation results under Rician fading channels show that the proposed system is capable of achieving promising BER performance while preserving the low power and low complexity advantages of ND-NOMA. This new ND-NOMA design enables simultaneous communication among three users using different dimensions, paving the way for scalable multi-user communication in noise-domain systems and in the IoT environments.

ÖZETÇE

Yeni Nesil Kablosuz Ağlar ve Nesnelerin İnterneti (IoT) Sistemleri için Gürültü Tabanlı İletişim

ERKİN YAPICI
Elektrik ve Elektronik Mühendisliği, Yüksek Lisans
7 Temmuz 2025

Kablosuz iletişimdeki mevcut gelişmeler, düşük veri hızlı Nesnelerin İnterneti (IoT) sistemleri için yeni fırsatlar açmıştır. Yüksek karmaşıklıkta işlemler üzerine kurulu sinyal işleme ve katı senkronizasyon gereksinimlerine dayanan eski iletişim çerçeveleri, modern ve gelecekteki IoT ağlarının temel gereksinimleri olan düşük bit hata oranı (BER), enerji toplama kabiliyeti ve düşük veri hızlarında güvenilir şekilde çalışabilme yeteneğini sıklıkla karşılayamamaktadır. Bu sınırlamaları gidermek için, veriyi deterministik olan frekans veya faz gibi parametreler yerine yapay olarak üretilen Gauss gürültüsünün istatistiksel özellikler olan, ortalama, varyans ve korelasyon parametrelerine kodlayan gürültü-temelli modülasyon teknikleri ortaya çıkmıştır. Bu yaklaşımlar güç tahsisi ihtiyacını ve ayrıca ardışık girişim iptalini (SIC) ortadan kaldırır, bu da karmaşıklığı ve enerji tüketimini azaltır. Daha açık ifade etmek gerekirse, senkronizasyon ve denkleştirme gereksinimini ortadan kaldırarak bu teknikler dinamik ve öngörülemeyen kablosuz ortamlarda uygun iletişim sağlar.

Bölüm, gelişmekte olan gürültü modülasyonu (Noise-Mod) tekniğinden yararlanarak gelecekteki Nesnelerin İnterneti (IoT) cihazları için yenilikçi bir birleşik enerji toplama (EH) ve iletişim şeması sunmaktadır. Önerilen yaklaşım, bilgiyi gerçek Gauss gürültüsü örneklerinin ortalama değerine gömerek kablosuz enerji ve bilgi toplama imkanı sağlar. Bilgiyi çözmek için ortalama-temelli bir algılayıcı öneriyoruz ve önerilen şemanın Rician solma kanallarındaki analitik bit hata olasılığını (BEP) türetiyoruz. Ayrıca, önerilen şemanın enerji toplama kabiliyeti açısından uygulanabilirliğini göstermek için doğrusal olmayan bir rektanna modeli kullanıyoruz. Simülasyon sonuçları, önerilen yöntemin çeşitli kanal koşullarında geleneksel modülasyon tekniklerine kıyasla enerji toplama performansını üstün şekilde gerçekleştirdiğini ve gelecek nesil IoT ağları için güvenilir iletişim performansını koruduğunu göstermektedir.

Bölümde, bilgiyi ortalama ve varyansın modülasyonu ile aktaran yenilikçi bir iletişim şeması olan gürültü-temelli ortogonal olmayan çoklu erişim (ND-NOMA) sunulmaktadır. Gücün farklı seviyelerine dayanan ve büyük ölçüde ardışık girişim iptaline (SIC) bağımlı geleneksel güç-temelli ortogonal olmayan çoklu erişim (PD-NOMA) yöntemlerinden farklı olarak, ND-NOMA gürültü alanını kullanır ve böylece güç tüketimini ve sistem karmaşıklığını önemli ölçüde azaltır. Gürültü modülasyonundan ilham alan ND-NOMA enerji verimliliğini artırır ve daha düşük bit hata oranları sağlar, bu da onu yeni nesil IoT ağları için son derece uygun hale getirir. Teorik analizlerimiz ve bilgisayar simülasyonlarımız, ND-NOMA'nın Rician solma kanallarında hem yükselen bağlantı hem de düşen bağlantı senaryolarında son derece düşük bit hata oranlarına ulaşabildiğini göstermektedir. Önerilen çok kullanıcılı sistem, ortalama tespiti için minimum mesafe algılayıcı ve varyans tespiti için eşik temelli algılayıcı ile desteklenmekte olup düşük güçlü ortamlarda sağlam iletişim sağlar. Gürültünün doğasında bulunan özelliklerden yararlanarak ND-NOMA, düşük maliyetli ve düşük karmaşıklıklı cihazların uzun vadeli konuşlanmaları için umut verici bir platform sunmaktadır.

Son olarak, 5. Bölümde, iki kullanıcılı ND-NOMA'da kullanılan ortalama ve varyans boyutlarına ek olarak korelasyonu yeni bir boyut olarak tanıtan yenilikçi bir üç kullanıcılı gürültü-temelli ortogonal olmayan çoklu erişim ND-NOMA şeması önerilmektedir. Yeni üç kullanıcılı ND-NOMA şeması, hem yükselen bağlantı hem de düşen bağlantı senaryolarını kapsamakta ve bilgiyi ortalama, varyans ve korelasyona gömerek kodlayan algılayıcılar tasarlamaktadır. Rician solma kanallarındaki teorik analizimiz ve simülasyon sonuçlarımız, önerilen sistemin umut verici bit hata oranı performansına ulaştığını ve ND-NOMA'nın düşük güç ve düşük karmaşıklık avantajlarını koruduğunu göstermektedir. Bu yeni ND-NOMA tasarımı, üç kullanıcının farklı boyutları kullanarak eşzamanlı iletişim kurmasını sağlamakta ve gürültü-temelli sistemlerde ölçeklenebilir çok kullanıcılı iletişimin önünü açarak IoT ortamlarında yeni bir dönemin kapılarını aralamaktadır.

ACKNOWLEDGMENTS

This thesis is dedicated to my supervisor, Professor Ertuğrul Başar, whose mentorship, trust, and support made this work possible. I am deeply grateful to him for giving me the opportunity to shine.

I also dedicate this work to the Yapıcı family, with special mention to İlkin, İnciser, M. Şükrü, and Hekime Yapıcı, for their unity and encouragement throughout my academic journey. We truly are a special family.

Thank you, Murat Akça, for being an inspiring leader and a true role model in life. You have truly made a big impact on my life.

To Selin Aksoy, thank you for standing by me with love and faith through every step of this journey. I couldn't have done it without you.

I would like to express my heartfelt gratitude to my grandmother, Emine Nuriye Meci. I know that you are watching over me and are proud of me.

To Yusuf İslam Tek, Ertuğ Pıhtılı, and all members of the CoreLab family; thank you for your collaboration, insights, and friendship.

To my beloved pet Gaguş, thank you for your comforting presence during long study nights.

TABLE OF CONTENTS

LIST OF TABLES

LIST OF FIGURES

ABBREVIATIONS

5G	Fifth Generation
6G	Sixth Generation
AWGN	Additive White Gaussian Noise
BEP	Bit Error Probability
BER	Bit Error Rate
BPSK	Binary Phase Shift Keying
BS	Base Station
CDF	Cumulativve Distribution Function
CLT	Central Limit Theorem
CPEP	Conditional Pairwise Error Probability
CSCG	Circularly Symmetric Complex Gaussian
CSI	Channel State Information
EH	Energy Harvesting
IEEE	Institute of Electrical and Electronics Engineers
IoT	Internet of Things
ISI	Inter-Symbol Interference
JEIH	Joint Energy and Information Harvesting
LoS	Line-of-Sight
MC	Monte Carlo
ML	Maximum Likelihood
ND-NOMA	Noise-Domain Non-Orthogonal Multiple Access
NoiseMod	Noise Modulation
NOMA	Non-Orthogonal Multiple Access

PAM	Pulse Amplitude Modulation
PD-NOMA	Power-Domain Non-Orthogonal Multiple Access
PS	Power Splitting
PSK	Phase Shift Keying
QAM	Quadrature Amplitude Modulation
RG	Real Gaussian
SIC	Successive Interference Cancellation
SNR	Signal-to-Noise Ratio
SWIPT	Simultaneous Wireless Information and Power Transfer
TS	Time Switching
UPEP	Unconditional Pairwise Error Probability

Chapter 1

INTRODUCTION

In the speedly evolving field of wireless communications, the push towards the 6G networks is accelerating the development of innovative techniques that address the demands of ultra-reliable, low-latency, and energy efficient connectivity. As the amount of IoT devices increases and applications such as smart cities become more widespread, the need for novel communication methods has never been greater.

Conventional modulation schemes, while effective in traditional scenarios, had some challenges under the contraints imposed by the next generation IoT use cases. In these IoT use cases, there were some limitations in energy availability, low-complexity device architecture, and the necessity for simultaneous energy and data transmission. To add on, many existing multiple access strategies, such as PD-NOMA rely on SIC technique that increase receiver complexity and degrade performance under imperfect channel conditions.

To overcome these challenges, promising research has explored alternative modulation domains and system architectures that utilize the statistical properties of noise signals. Among these alternative modulation domains, NoiseMod has been a promising candidate duo to its ability to embed information in the mean, variance, or correlation of the Gaussian noise samples. This innovative paradigm enables energy efficient communication and supports simple receiver designs, which are ideal for constrained IoT environments.

Building on this foundational research, ND-NOMA has been proposed as a low complexity alternative to conventional NOMA schemes, eliminating the need for SIC by simultaneously encoding user data in distinct noise domain features. Additionally, joint energy and information harvesting using Gaussian noise signals offers a promising future to the power batteryless IoT devices while maintaining reliable data transmission.

This thesis introduces three frameworks enhancing the noise domain communication: a mean based joint energy information harvesting scheme, a two-user ND-NOMA using mean and variance modulation, and a new three user ND-NOMA scheme using correlation, mean and variance; targeting efficient, low complexity IoT communication.

1.1 Contributions

Firstly, we propose an innovative joint energy and information harvesting (JEIH) scheme based on mean modulated Gaussian noise, and it is called JEIH-Noise Mod. In this framework, information bits are encoded into the mean of real Gaussian noise samples, enabling low complexity mean based detection at the receiver. The transmission is being operated in a time-switching manner, where a portion of each bit interval is dedicated to energy harvesting using a nonlinear rectenna model. Analytical expressions for the bit error probability (BEP) are derived under Rician fading conditions. Simulation results indicate that JEIH-Noise Mod achieves reliable communication while enhancing energy harvesting capability compared to concentional schemes, making it suitable for next-generation low-power IoT applications.

Secondly, we propose a two-user ND-NOMA scheme, where each user's data is embedded into a distinct statistical property of the Gaussian noise. In this work, it is mean and variance respectively for User 1 (U_1) and User 2 (U_2). In this work, the separation thus eliminates the need for SIC, enabling a simple yet low BER multiple access framework. The mean modulated user employs a minimum distance detector, on the other hand variance modulated user employs a variance threshold detector. Analytical BEP expressions are derived under Rayleigh and Rician fading conditions, and simulations validate the system's low complexity and high reliability performancce. Our proposed scheme demonstrates significant potential for energy efficient, low data rate communication in future IoT environments.

Finally, we propose a new ND-NOMA framework to support three users by introducing correlation as a third independent modulation dimension, in addition to mean and variance. In this new system, each user encodes data using one of the three noise domain properties: mean, variance or the correlation of Gaussian noise samples. A distinct detection architecture is designed, where each user's signal is extracted using a dimension specific simple detector without requiring any interference cancellation technology. Theoretical BEP analyses are provided for all users under Rician fading, and simulation results confirms that the proposed three user ND-NOMA system maintains reliable performance under various Rician channel condition. This contribution holds the potential to provide multi-user, lower-power communication in dense IoT environments.

Chapter 2

NOISE MODULATION

NoiseMod is a novel communication paradigm that, unlike traditional systems which treat noise as a harmful effect, utilizes noise itself as an information carrier. Instead ofmodulating the amplitude, frequency, or phase of a high-frequency carrier signal, NoiseMod encodes digital information into the statistical parameters of noise, like mean, variance, or correlation. The concept is categorized into two schemes: TherMod, which leverages inherent thermal noise from passive components like resistors, and external NoiseMod, which employs artificially generated and modulated noise signals. For instance at the receiver, the signal is downconverted and samples, and the sample variance is computed to extract the embedded information using a threshold-based detector. This approach enables non-coherent detection, time diversity, and even ultra-low power communication, making it attractive for covert and secure wireless systems.

2.1 A Literature Survey on Noise Modulation

Back in foundational research, to carry information, thermal noise modulation (TherMod) was introduced [Kish, 2005, Basar, 2024]. On top of this foundational concept, subsequent studies proposed modulating information through the statistical parameters of the noise signal itself, such as the variance or mean [Basar, 2024, Kish, 2006, Kramer and Bessai, 2017, Basnayaka and Haas, 2017, Kozlendrakov and Boysi, 2018, Anand, 2019, Yapici et al., 2025]. These studies jointly demonstrate that noise modulation has the potential for simplifying receiver design, increasing robustness towards the channel imperfections, achieving covert and secure communications, enabling low complexity communication. Specifically, certain noise modulation forms allow for non-coherent detection, where the receiver can extract information solely by estimating signal statistics such as variance, without the need of any knowledge of the instantaneous channel state. Furthermore, phase and frequency synchronization is not required in these schemes, which significantly reduces the receiver complexity. To add on, by distributing the noise samples corresponding to a single information bit across multiple time slots, noise modulation inherently enables time diversity, which enhances robustness in fading environments without requiring complex combining techniques or multiple antennas. Finally, noise-alike waveforms provide significant advantages in terms of secure and covert communications. These features make noise modulation suitable for low-data-rate scenarios, where minimizing receiver complexity and maximizing energy efficiency are critical. Building on this foundation and the fascinating property of the Gaussian distribution, where the sum of two independent Gaussian variables remains Gaussian [Ding et al., 2014], our prior work introduced a two-user noise-domain non-orthogonal multiple access (ND-NOMA) scheme, where user information was encoded through the mean and variance of artificially generated noise, offering a promising solution for emerging energy-constrained applications [Yapici et al., 2024, Butt et al., 2024]. Distinct from PD-NOMA schemes that rely heavily on SIC, ND-NOMA inherently avoids the need for such complex receiver operations by employing statistical noise parameters for information encoding. Moreover, as the scheme operates purely in the noise domain, it eliminates the requirement for precise frequency and phase synchronization, further reducing receiver complexity and making it highly attractive for low-data-rate applications. On the other hand also, ND-NOMA system has a simple detection structure thus it avoids typical error propagation problems which we observe in PD-NOMA systems. This foundational progression sets the stage for our current work, where we reshape the ND-NOMA paradigm to support a third user by leveraging correlation as a new statistical dimension, thereby enhancing the scalability and flexibility of noise-domain communication. It is worth noting that some earlier schemes considered correlation to carry information in secure and covert noise-driven communications, but not in the context of multiple accessing [Salbert and Hanssen, 1999, Xu et al., 2017].

NoiseMod operates by embedding digital bits into the variance levels of Gaussian

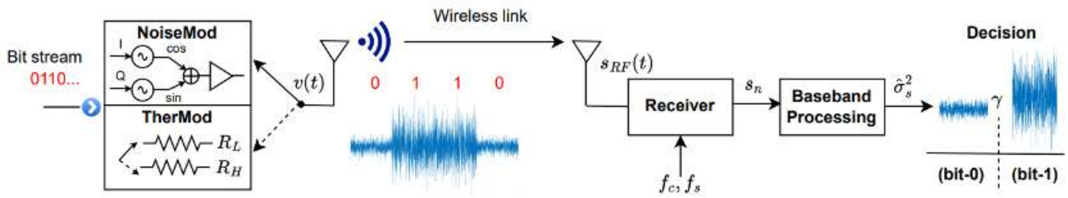

Figure 2.1: Transceiver architecture of noise modulation. $v(t)$: thermal or externally-generated noise waveform, $s_{RF}(t)$: received signal scaled by a complex factor due to channel, f_c/f_s: carrier/sampling frequency. For NoiseMod, $v(t) = \Re\left\{u(t)e^{j2\pi f_c t}\right\}$ with $u(t)$ being the complex baseband noise waveform [Basar, 2024].

noise signals, leveraging a simple yet effective transceiver design as illustrated in Figure 2.1. During each bit duration, the transmitter emits noise samples with either low or high variance depending on the bit value. Specifically, a bit-0 is represented by a noise waveform with variance σ_0^2, while a bit-1 corresponds to a higher variance $\sigma_1^2 = \alpha\sigma_0^2$. At the receiver, the complex baseband samples s_n are used to estimate the sample variance as

$$\hat{\sigma}^2 = \frac{1}{N}\sum_{n=1}^{N}|s_n|^2,$$

which is then compared to a predefined threshold γ to make a binary decision:

$$\hat{b} = \begin{cases} 0, & \hat{\sigma}^2 < \gamma \\ 1, & \hat{\sigma}^2 \geq \gamma \end{cases}$$

This simple threshold-based detection scheme does not require knowledge of the instantaneous channel state, thus allowing non-coherent operation. The system design and performance analysis for this approach are extensively detailed in [Basar, 2024].

Chapter 3

NOISE MODULATION OVER WIRELESS ENERGY TRANSFER: JEIH-NOISE MOD

In this chapter we present an innovative joint EH and communication scheme for future IoT devices by leveraging the emerging noise modulation NoiseMod technique. The proposed approach embeds information into the mean value of real Gaussian noise samples to enable wireless energy and information harvesting. We propose a mean-based detector to decode the information and derive the analytical BEP of the proposed scheme under Rician fading channels. We utilize a nonlinear rectenna model to demonstrate the feasibility of the proposed scheme in terms of energy harvesting capability. Simulation results demonstrate that the proposed method outperforms conventional modulation techniques in terms of EH performance across various channel conditions while maintaining reliable communication performance for next-generation IoT networks.

This chapter is structured as follows. Section 3.1 presents the detailed system model for both information transmission and energy harvesting. Section 3.2 provides a theoretical analysis of the BEP expressions. Section 3.3 discusses simulation results for both BER and energy harvesting performance.

3.1 JEIH-Noise Mod System Model

In this section, we present the transceiver architecture of the proposed JEIH-Noise Mod scheme that is illustrated in Fig. 3.1. We consider a total number of N samples per bit duration for joint energy and information harvesting, employing the TS mode as the operation mode [Zhou et al., 2013]. In the TS mode, during the first $N_e = \alpha N$ samples, the information harvester is inactive, and the entire signal power is dedicated to energy harvesting, where α is the portion of time that the energy

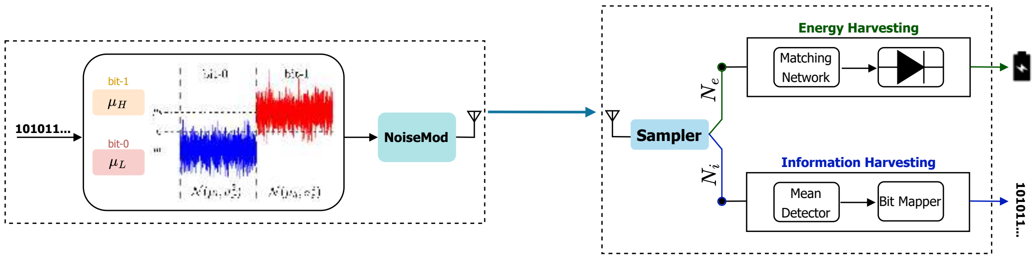

Figure 3.1: Transceiver scheme of the proposed JEIH-Noise Mod system. Bits are mapped into mean and variance of Gaussian noise in the transmitter and energy harvesting/information harversting are implemented in the receiver, respectively.

harvester is active. For the remaining $N_i = (1-\alpha)N$ samples, the information harvester is active, and all signal power is utilized for information decoding. In this proposed scheme, the mean value of the RG noise samples is modulated to encode information. Therefore, this scheme utilizes noise samples with a fixed variance and controllable mean to simultaneously facilitate information transfer and energy harvesting.

3.1.1 Information Harvesting

The transmission of bit-b (bit-0 or bit-1) is realized using N_i consecutive, randomly generated Gaussian noise samples, and a sample is defined as $x_n \sim \mathcal{N}(\mu, \sigma_x^2)$, , where $n = 1, \ldots, N_i$, μ and σ_x^2 denote the corresponding mean value for bits and the variance of the noise samples (i.e., serves as the overall transmit power factor). μ is selected as follows:

$$\mu = \begin{cases} \mu_l, & \text{if bit-0 is transmitted,} \\ \mu_h, & \text{if bit-1 is transmitted,} \end{cases} \tag{3.1}$$

Herein, $\mu_l = -m$ and $\mu_h = +m$ represent the symmetric mean values corresponding to bit-0 and bit-1, respectively. Under the transmit power constraint, $\Sigma_{n=1}^{N_i}\mathbb{E}[x_n^2] = \mu^2 + \sigma_x^2 = P_T$, where P_T is normalized to unit power, this symmetric mean selection ensures equal average transmit power for each bit.

Afterward, we express the n-th received complex baseband sample y_n over a wireless channel as

$$y_n \;=\; h\, x_n \;+\; w_n, \tag{3.2}$$

where $w_n \sim \mathcal{CN}(0,\, \sigma_w^2)$ corresponds to additive white Gaussian noise (AWGN) sample with variance σ_w^2. Additionally, for a forthcoming analysis to evaluate the error performance of the system, we define $\delta = \sigma_x^2/\sigma_w^2$, which represents the ratio of variances between the useful signal and the additive Gaussian noise components. This parameter is analogous to the signal-to-noise ratio (SNR) in conventional digital communication systems. A higher value of δ indicates increased robustness of the receiver against the effects of additive disruptive noise, leading to a lower bit error probability (BEP). Moreover, $h = \bar{h}/\sqrt{L}$ is the complex baseband channel coefficient of the transmitter and receiver link. Here, L denotes the attenuation due to the distance between the transmitter and receiver, and it is calculated as

$$L = \left(\frac{4\pi\, d\, f_c}{c}\right)^2, \tag{3.3}$$

where d, f_c, and c correspond to the distance in meters, carrier frequency, and the speed of light, respectively. Furthermore, $\bar{h} = \bar{h}_R + j\bar{h}_I$ is the small-scale channel coefficient for Rician fading with parameter K and $\bar{h}_R, \bar{h}_I \sim \mathcal{N}\left(\sqrt{\frac{K}{2(1+K)}}, \frac{1}{2(1+K)}\right)$. $\bar{h}$ is normalized to have unit gain in average, i.e. $\mathbb{E}[|\bar{h}|^2] = 1$. Furthermore, we assume block fading, that is h remains constant during each transmission (bit) interval.

At the receiver, the sample mean estimation of the received signals is computed to decode the information bits as

$$\bar{y} = \frac{1}{N_i} \sum_{n=1}^{N_i} y_n. \tag{3.4}$$

The estimated information bit, $\hat{b}$, is detected using the minimum distance rule, which is formulated as

$$\hat{b} = \begin{cases} 0, & \text{if} \quad |\bar{y} - h\mu_l|^2 < |\bar{y} - h\mu_h|^2 \\ 1, & \text{if} \quad |\bar{y} - h\mu_h|^2 < |\bar{y} - h\mu_l|^2. \end{cases} \tag{3.5}$$

3.1.2 Energy Harvesting

In the EH phase, N_e Gaussian noise samples are fed to the rectenna to scavenge energy from received Gaussian signals. The harvested power can then be used directly or stored in a battery. A rectenna, consisting of an antenna and a rectifier, plays a crucial role in the EH process. The rectifier specifically converts the received radio frequency (RF) power into DC power. Herein, we employ a single-diode rectifier model. After passing through a matching network, which ensures impedance matching between the antenna and the rectifier, the single-diode rectifier converts the received Gaussian noise samples into DC power as shown in Fig. 3.1. To account for the practical characteristics of the rectenna based on design preferences, the authors in [Clerckx and Bayguzina, 2016] proposed a nonlinear rectenna model. This model exploits the Taylor series expansion of the diode characteristic function to investigate the effect of different signaling/modulation schemes on the system's energy harvesting capability. This expression is mathematically given by,

$$z_{\mathrm{DC}} = k_2 R_{\mathrm{ant}} \mathbb{E}[|y_n|^2] + k_4 R_{\mathrm{ant}}^2 \mathbb{E}[|y_n|^4], \tag{3.6}$$

where k_2 and k_4 are rectifier-dependent parameters, and R_{ant} represents the antenna impedance.

Unlike conventional linear rectenna models, where the energy harvesting capability depends only on the received power and not on the utilized waveform, [Pihtili et al., 2024] highlights the influence of different waveforms on the system's energy harvesting capability. The term $\mathbb{E}[|y_n|^2]$ represents the linear component and depends exclusively on the received power, while $\mathbb{E}[|y_n|^4]$ accounts for the nonlinear characteristics of the rectenna and varies with the type of transmit signal [Clerckx and Bayguzina, 2016]. Thus, using RG signals instead of CSCG or linear modulated ones is beneficial for energy harvesting, as indicated in [Kim et al., 2020]. However, using the mean of RG signals for information harvesting affects the system's energy harvesting capability. Under the transmit power constraint $\sum_{n=1}^{N_e} \mathbb{E}[x_n^2] = \mu^2 + \sigma_x^2 = P_T$, where P_T is normalized to unit power, increasing the mean parameter μ reduces the variance σ_x^2 accordingly. This reduction diminishes the amplitude fluctuations of the RG signal, thereby reducing the energy harvesting capability, whereas waveforms with amplitude fluctuations are beneficial for enhancing energy harvesting capability [Pihtili et al., 2024, Clerckx and Bayguzina, 2016].

3.2 Error Analysis

In this section, we derive the theoretical BEP expressions for the proposed scheme. We assume that the channel is perfectly known at the receiver in this analysis, as well as in computer simulations.

At the receiver, we can further express the sample mean $\bar{y}$ in (3.4) as

$$\bar{y} \;=\; \frac{1}{N_i}\sum_{n=1}^{N_i} y_n \;=\; h\bar{x} \;+\; \bar{w}, \tag{3.7}$$

where $\bar{x} = \frac{1}{N_i}\sum_{n=1}^{N_i} x_n$ and $\bar{w} = \frac{1}{N_i}\sum_{n=1}^{N_i} w_n$. In order to simplify the analysis, we exploit a standard trick of removing the complex phase of the channel. Let us rewrite complex baseband channel coefficient h as $h = r\,e^{j\phi}$, and ϕ is the phase of the channel. By removing the phase, we have

$$\widetilde{y} \;=\; e^{-j\phi}\bar{y}, \tag{3.8a}$$

$$\widetilde{w} \;=\; e^{-j\phi}\bar{w}, \tag{3.8b}$$

$$r \;=\; e^{-j\phi}h. \tag{3.8c}$$

Since AWGN is circularly symmetric, $\widetilde{w} \sim \mathcal{CN}(0, \sigma_w^2/N_i)$ has the same distribution as $\overline{w}$. We have the rotated sample mean signal $\widetilde{y}$, which can be expressed as follows

$$\widetilde{y} = r\bar{x} + \widetilde{w}, \tag{3.9}$$

where $\bar{x}$ follows $\mathcal{N}(\mu_l, \sigma_x^2/N_i)$. For $b = 0$, an error occurs when error event below holds,

$$|\widetilde{y} - r\mu_h|^2 < |\widetilde{y} - r\mu_l|^2. \tag{3.10}$$

It can be shown that the error event in (3.10) can be rewritten as a threshold condition on a real Gaussian variable

$$z \;=\; r\;(\overline{x} - (-\,m)) \;+\; \Re\{\widetilde{w}\}. \tag{3.11}$$

Let us define an auxiliary variable such that $\omega = \mu_h - \mu_l = 2m$. Then $z \sim \mathcal{N}\big(0,\ \frac{r^2\sigma_x^2}{N_i} + \frac{\sigma_w^2}{2N_i}\big)$. Conditioned on amplitude r, the instantaneous probability of error is

$$\Pr(\text{error} \mid b = 0, r) = \Pr\big\{z > \tfrac{1}{2} r\omega\big\} = Q\left(\frac{\frac{1}{2} r\omega}{\sqrt{\frac{r^2\sigma_x^2}{N_i} + \frac{\sigma_w^2}{2N_i}}}\right). \tag{3.12}$$

By symmetry, the same holds for $b = 1$. Since $\bar{h}$ has unit second moment, $|\bar{h}|$ follows a Rician distribution with probability density function (pdf)

$$f_{|\bar{h}|}(x) \;=\; \frac{x}{\sigma_s^2}\, \exp\!\left(-\frac{x^2 + s^2}{2\,\sigma_s^2}\right) I_0\!\left(\frac{x\, s}{\sigma_s^2}\right), \quad x \geq 0, \tag{3.13}$$

where $s^2 + 2\,\sigma_s^2 = 1$ and $K = \frac{s^2}{2\,\sigma_s^2}$. With path loss L, we get $r = x/\sqrt{L}$. Therefore, the scaled Rician pdf can be expressed as

$$f_r(r) = \left(\frac{\sqrt{L}\, r}{\sigma_s^2}\right) \exp\!\left(-\frac{L\, r^2 + s^2}{2\,\sigma_s^2}\right) I_0\!\left(\tfrac{r\sqrt{L}\, s}{\sigma_s^2}\right), \quad r \geq 0. \tag{3.14}$$

Finally, we average Q function in (3.12) over the distribution of r, and the unconditional BEP is found below

$$P_{\mathrm{e}} \;=\; \int_0^{\infty} Q\left(\frac{rm}{\sqrt{\frac{1}{2N_i}\left(2r^2\sigma_x^2 + \sigma_w^2\right)}}\right) f_r(r)\, \mathrm{d}r. \tag{3.15}$$

We numerically evaluate the integral in (3.15) with the adaptive quadrature method [Press, 2007].

3.3 JEIH-Noise Mod Simulation Results

In this section, we validate the analytical BER derivations and show the energy harvesting capability based on (6) through computer simulations. The theoretical BEP curves are obtained from (3.15). Table 3.1 summarizes the simulation parameters, including antenna impedance, rectifier coefficients, carrier frequency, and TS factors.

3.3.1 Energy Harvesting Capability

Fig. 3.2 illustrates the energy harvesting capability, denoted as z_{DC}, for diverse modulation schemes, including the TS and PS modes of the proposed JEIH-Noise Mod,

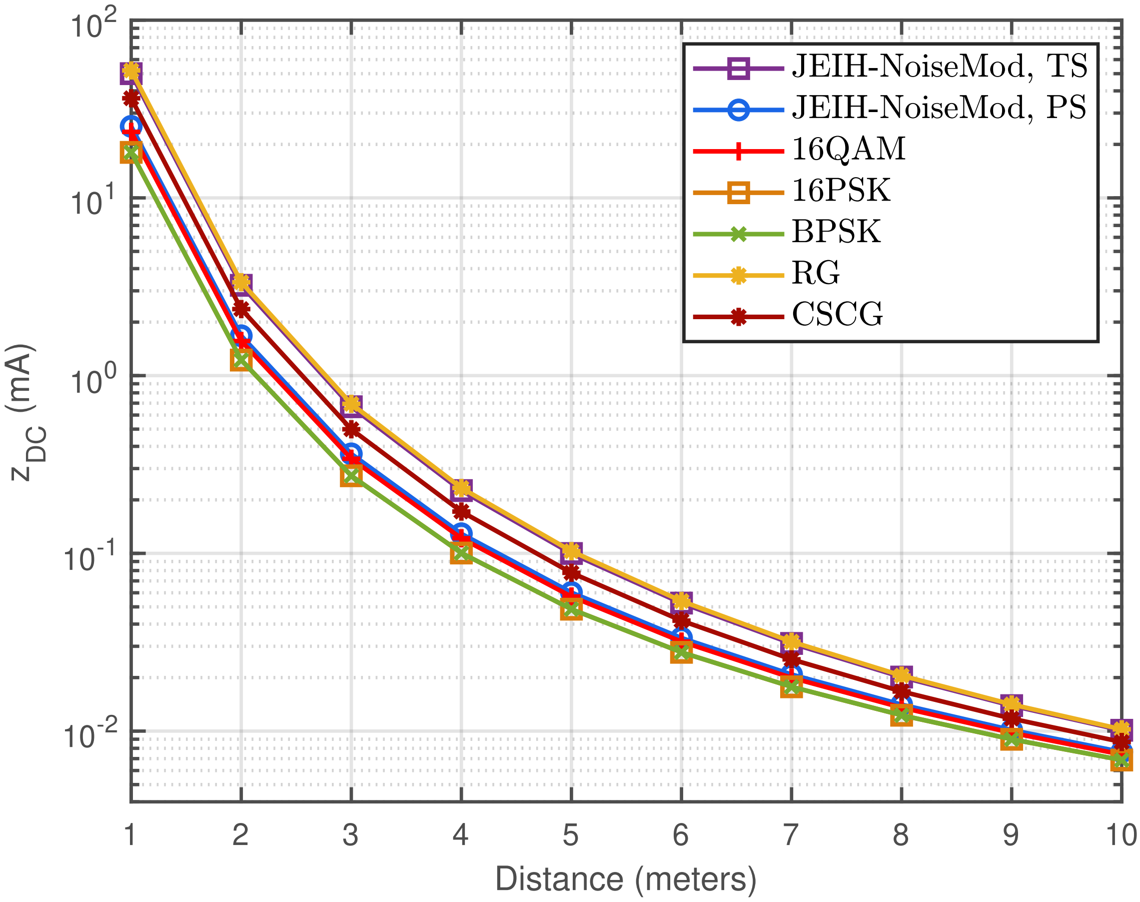

Figure 3.2: Energy harvesting capability (z_{DC}) vs. distance for different modulation schemes.

16-QAM, 16-PSK, BPSK, RG, and CSCG signals. In the PS baseline scenario, the signal power is divided with a power-splitting factor of ρ for energy harvesting and $1-\rho$ for information harvesting through the power divider block before the sampling process. In this simulation, we set $N_e = 100$. The proposed JEIH-Noise Mod scheme significantly improves energy harvesting capability, particularly at shorter distances. As expected, when the distance increases due to the path loss effect, the energy harvesting capability decreases for all modulation schemes. However, JEIH-Noise Mod in TS mode consistently outperforms conventional modulation schemes. Notably, its performance is comparable to RG, which is considered ideal for energy harvesting.

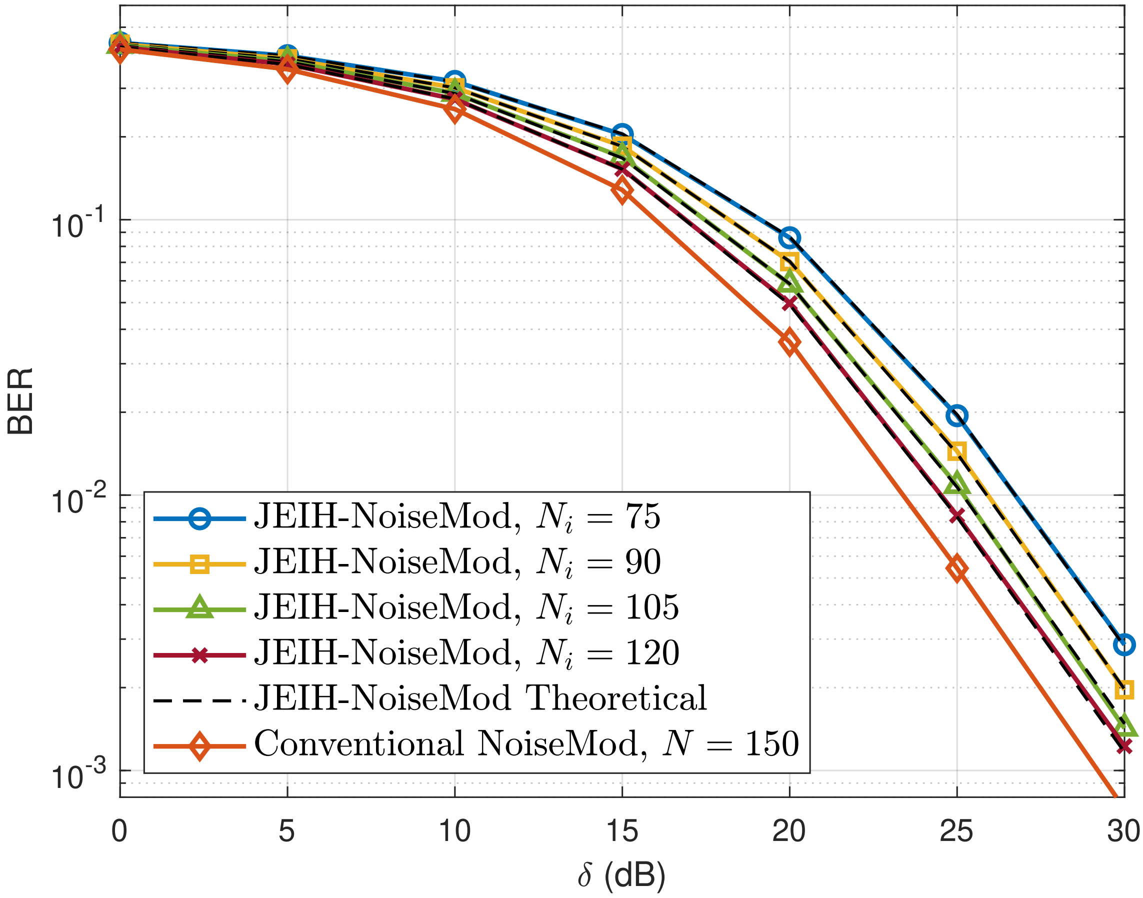

Figure 3.3: δ versus theoretical and simulated BER for varying N_i values .

3.3.2 Error Performance

Fig. 3.3 illustrates the BER performance as a function of the variance ratio δ for different values of N_i. We choose $K = 5$, $d = 3\,\text{m}$ and use the α values from Table 3.1, where the N_i values are set to match the corresponding α values. As N_i increases, the BER improves significantly due to the more accurate averaging of noise samples. Expectedly, $N_i = 120$ achieves the lowest BER across all δ values, demonstrating the benefits of processing more samples for reliable detection. Compared with the conventional NoiseMod scheme and our proposed scheme JEIH-Noise Mod with $N_e = 120$, there is a slight difference in terms of error performance. The reason for the slight difference is due to the number of noise samples; for the JEIH-Noise Mod cases, N_i was used, which splits the N accordingly. Expectedly, since N is not split and is used only for information reception in conventional NoiseMod, a difference

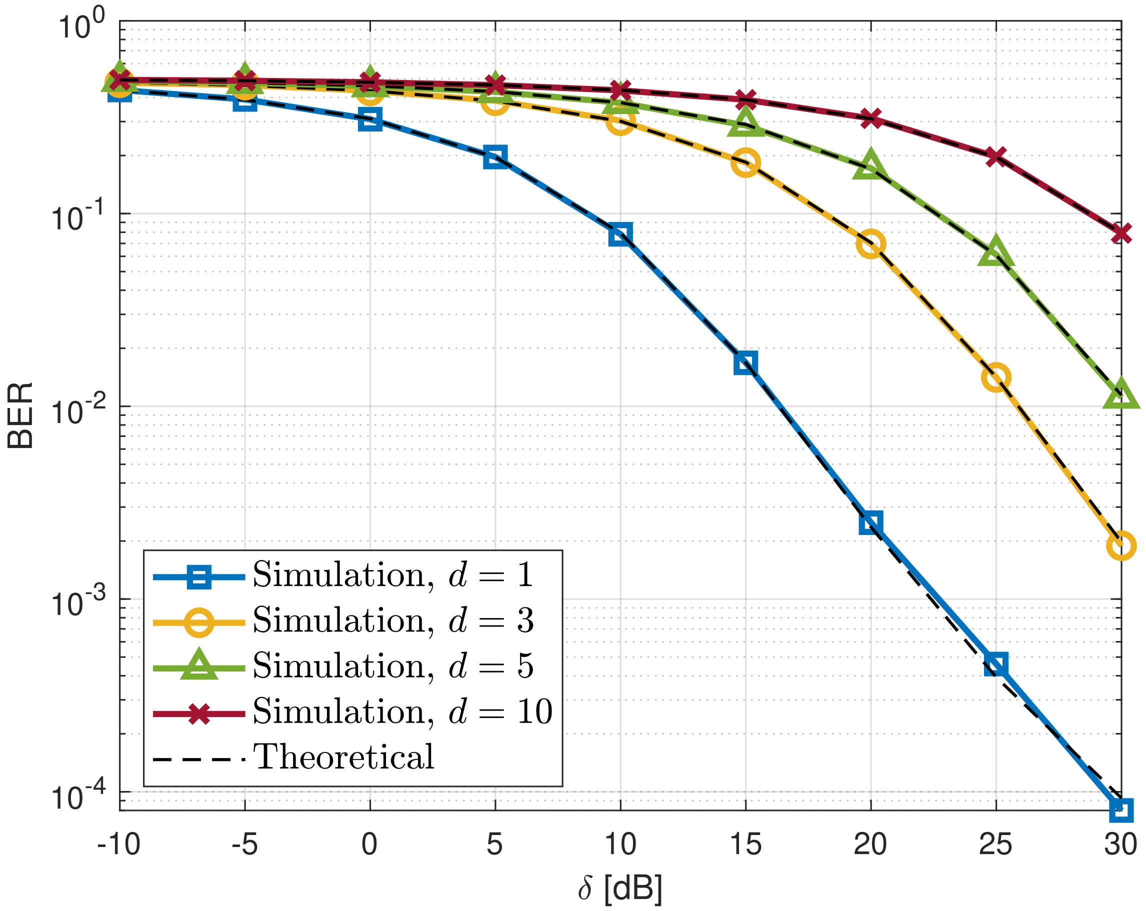

Figure 3.4: δ versus theoretical and simulated BER for varying distances.

can be observed for various N_i values that are less than N. Furthermore, NoiseMod uses mean values to carry information.

The BER performance for varying transmitter-receiver distances d for $K = 5$ is illustrated in Fig. 3.4 to demonstrate the effect of increasing path loss on the JEIH-Noise Mod scheme. Shorter distances result in better BER performance due to reduced path loss and stronger received signal power, where the proposed scheme showcases reasonable energy harvesting capability. The BER performance degrades as the distance increases, with $d = 10$ meters showing the highest BER across all δ values. Moreover, the theoretical and simulated results align closely, validating our analytical expressions.

The impact of the Rician fading parameter K on the BER performance is evaluated in Fig. 3.5, where $d = 3$ m and $N_i = 90$ samples are used. Higher values

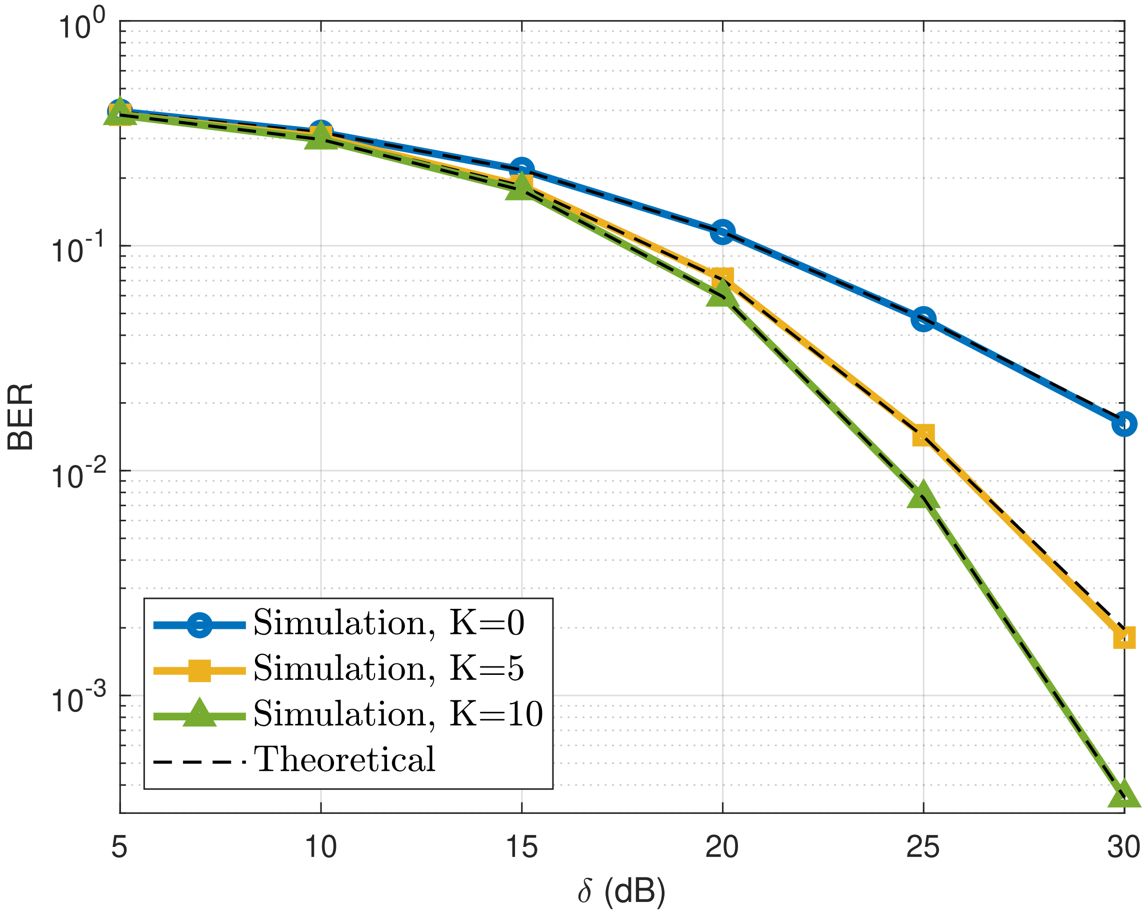

Figure 3.5: δ versus theoretical and simulated BER for varying Rician K-factor values.

of K, indicating a stronger line-of-sight (LoS) component, result in improved BER performance. For $K = 10$, the system achieves the lowest BER, demonstrating the advantage of a dominant LoS channel. When $K = 5$, the proposed system maintains satisfactory error performance. Notably, even in the absence of an LoS component ($K = 0$), the system ensures reliable communication, highlighting its robustness under severe multipath conditions.

The impact of channel estimation errors on the BER performance is illustrated in Fig. 3.6for distances of $d = 1\,\mathrm{m}$ and $d = 3\,\mathrm{m}$ under different estimation error variances σ_e^2. In computer simulations, we set $K = 5$ and $N_i = 90$ samples are used. The imperfect CSI is modeled as $\hat{h} = h + \epsilon, \quad \epsilon \sim \mathcal{CN}(0, \sigma_e^2)$, and $\hat{h}$ is used instead of h in(3.5). As σ_e^2 increases, only slight BER degradations are observed across all

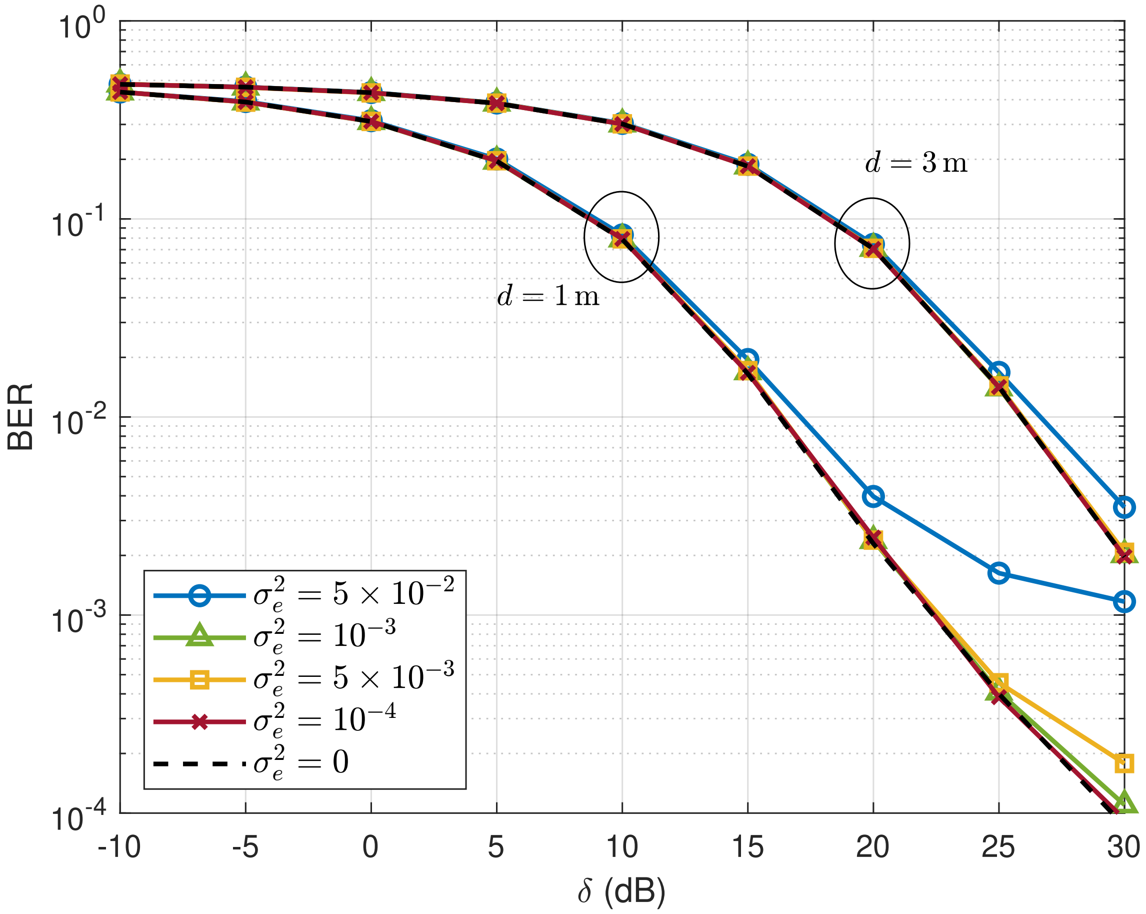

Figure 3.6: δ versus theoretical and simulated BER for varying σ_e^2 values.

δ values, demonstrating that the proposed JEIH-Noise Mod scheme remains robust even with channel estimation errors. This resilience arises from our simple threshold-based detection rule (3.5), which relies on the sample mean rather than precise channel amplitude estimates. Thus, erroneous channel coefficients have minimal impact on the decision metric. The close alignment between the perfect CSI and imperfect CSI curves confirms that the mean detector effectively mitigates the effect of estimation errors across varying distances.

Despite the inherently low bit rate characteristic of backscatter communication and IoT-based systems [F. Jameel and Lee, 2019], our proposed scheme effectively integrates both information and energy harvesting without compromising performance. This demonstrates its ability to ensure reliable data transmission while benefiting from Gaussian signaling for energy harvesting, making it a suitable choice for

Table 3.1: Simulation Parameters

Parameter	**Value**
R_{ant} $[\Omega]$ [Kim et al., 2020]	50
k_2, k_4 [Kim et al., 2020]	$0.0034, 0.3829$
f_c [MHz]	433
N [samples]	150
d [m]	$[1, 10]$
μ_H, μ_L	$\sqrt{0.5}, -\sqrt{0.5}$
α	$0.2, 0.3, 0.4, 0.5$
σ_x^2	1
ρ	0.5

low-power applications. Consequently, by utilizing the NoiseMod scheme, the proposed system maintains strong energy harvesting capability and error performance, showcasing its potential for future energy-constrained IoT applications.

Chapter 4

NOISE-DOMAIN NON-ORTHOGONAL MULTIPLE ACCESS

In this chapter, by taking the noise modulation concept one step further, we propose an innovative communication scheme called ND-NOMA. The fascinating property of the Gaussian distribution is that the sum of two independent Gaussian variables remains Gaussian [Ding et al., 2014]. In ND-NOMA, we exploit this by adding two Gaussian noise signals, each carrying different user information. The resulting signal retains its Gaussian nature, simplifying processing and detection at the receiver, which allows the ND-NOMA to efficiently handle multiple signals with minimal error, ideal for low-power IoT networks. This scheme utilizes the mean and variance of the artificial noise signals to transmit data. Basically, bits of one user are modulated using the mean of the noise samples, while bits of the other user are modulated using the variance of the noise samples. Since ND-NOMA leverages noise samples, the system does not require processing steps such as frequency synchronization and equalization for the downlink scenario. Thus, ND-NOMA significantly reduces power consumption and system complexity, making it ideal for the low power consumption requirements of next-generation applications such as Internet-of-things (IoT) networks. Our theoretical analysis and computer simulations demonstrate that ND-NOMA can achieve exceptionally low bit error rate (BER) in both uplink and downlink scenarios. The robust performance of the system is supported by a minimum distance detector for mean detection and a threshold-based detector for variance detection, ensuring reliable communication even in low-power scenarios. Our findings indicate that ND-NOMA has excellent performance, particularly in Rician fading channels, and can be utilized for long-term and large-scale deployments of low-cost, low-complex devices.

In emerging IoT use-cases, legacy systems were not performing well enough in terms of scalability, so the low-data-rate communication schemes were essential. Unlike PD-NOMA or CD-NOMA, designed for high-throughput scenarios, ND-NOMA offers a noise-domain access strategy well suited for low-data-rate IoT environments. As next-generation multiple access technology is a key candidate for 6G, ND-NOMA aligns well with the access needs of future wireless communication scenarios. ND-NOMA is well-suited for integration with Device B types of ambient IoT systems, as highlighted in [Butt et al., 2024]. Device B, with its limited energy storage and semi-passive operation, aligns with ND-NOMA's low-power and low-complexity demands, essential for sustainable IoT deployments. For Device Type B, the goal is to have low complexity, and with its simple receiver architecture, ND-NOMA is well suited for low-data-rate scenarios (0.1–5 kbps). Device B is semi-passive, uses backscattering with limited energy storage, and has power consumption below 1 mW. By utilizing noise mean and variance and its low-complex receiver structures for data transmission, ND-NOMA reduces the need for power-intensive processes like synchronization, making it ideal for energy-efficient systems. Its robustness in low-power scenarios further enhances the performance of ambient IoT networks, positioning ND-NOMA as a strong contender for next-generation applications. Studies in ISAC show that random waveforms enhance spectral efficiency, complementing ND-NOMA's goals of low-power communication [Koivunen et al., 2024]. Moreover, energy harvesting techniques such as SWIPT further support ND-NOMA's energy-efficient design [Song et al., 2014, Ashraf et al., 2021]. As illustrated in Fig. 4.1, the ND-NOMA scheme is not designed for broadband cellular communication scenarios, but instead it is designed for low-power and low-data-rate IoT environments, and our main motivation is to decompose the signals without using SIC.

The remainder of ths section is organized as follows: Section 4.1 covers uplink ND-NOMA theory and BEP optimization, Section 4.2 addresses downlink performance, and Section 4.3 presents numerical results.

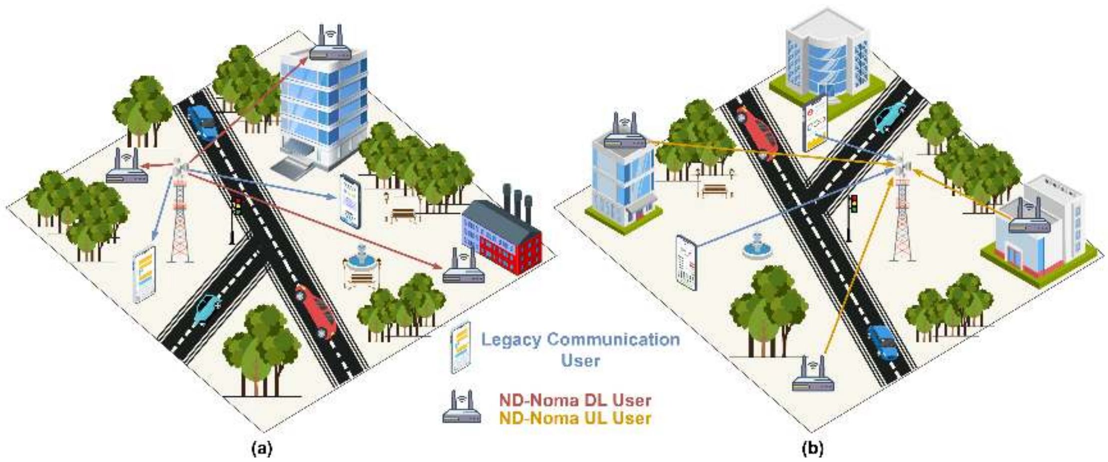

Figure 4.1: Illustration of a potential ND-NOMA use-case in low-data-rate, low-energy IoT environments, where (a) represents the downlink transmission and (b) represents the uplink transmission.

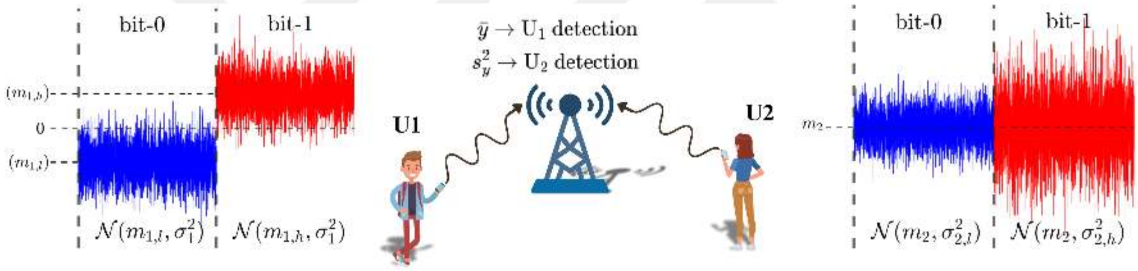

Figure 4.2: Uplink ND-NOMA scheme with two users using real Gaussian signals.

4.1 Uplink ND-NOMA: System Model and Performance Analysis

In this section, we first provide the system model for uplink ND-NOMA for two users and then introduce a general framework to assess the theoretical BEP performance of the two users.

4.1.1 System Model

As shown in Fig. 4.2, in the uplink transmission of two users, one of the users (User 1, U_1) uses the mean of the transmitted Gaussian samples. In contrast, the other user (User 2, U_2) exploits the variance as in noise modulation schemes. Specifically, denoting the nth noise samples of U_1 and U_2 respectively by s_1^n and s_2^n, for U_1, the transmission of information bits is accomplished by alternating the mean of the samples between low and high values, that is, for bit-0 and bit-1, we have, $s_1^n \sim \mathcal{N}(m_{1,l}, \sigma_1^2)$ and $s_2^n \sim \mathcal{N}(m_{1,h}, \sigma_1^2)$. As discussed later, we set $m_{1,h} = -m_{1,l}$ for optimum performance. We assume that two users consider N noise samples for each bit.

On the other hand, for U_2, we apply noise modulation by alternating the noise variance only, and for bit-0 and bit-1, we have $s_2^n \sim \mathcal{N}(m_2, \sigma_{2,l}^2)$ and $s_2^n \sim \mathcal{N}(m_2, \sigma_{2,h}^2)$. At this point, we set the mean of samples to zero, that is, $m_2 = 0$, to minimize the interference to U_1. This initial model assumes binary-level signaling, while a generalization is subject to further studies.

In this setup, we assume an average transmission power of P for each user, which corresponds to the second moment of the transmitted samples[1]: $E[(s_1^n)^2] = E[(s_2^n)^2] = P$, which equals to the sum of squared mean and variance of their samples. In light of this, $P = m_{1,l}^2 + \sigma_1^2$ for U_1. Here, U_1 dedicates β portion of its available power for the variance of its samples while dedicating a $(1-\beta)$ portion for the mean, that is, $\sigma_1^2 = \beta P$ and $m_{1,l}^2 = m_{1,h}^2 = (1-\beta)P$. Since $m_2 = 0$, all power of U_2 is dedicated to the variance of its samples, $P = (\sigma_{2,l}^2 + \sigma_{2,h}^2)/2$.

In what follows, we use the terminology considered in the study of [Basar, 2023] and define $\delta = \sigma_{2,l}^2/\sigma_w^2$ as the ratio of useful and disruptive noise variances. Additionally, α stands for the ratio of high and low variance values for U_2, that is, $\sigma_{2,h}^2 = \alpha\sigma_{2,l}^2$. Accordingly, we obtain $\eta = \sigma_1^2/\sigma_w^2 = (1+\alpha)\delta\beta/2$.

In light of the model in Fig. 4.2, the received nth noise sample at the receiver is expressed as

$$y^n = h_1 s_1^n + h_2 s_2^n + w^n, \quad n = 1, \ldots, N. \tag{4.1}$$

Here, h_1 and h_2 are the complex baseband channel coefficients of the links between U_1-base station (BS) and U_2-BS, respectively, and $w^n \sim \mathcal{CN}(0, \sigma_w^2)$ is the complex baseband additive white Gaussian noise sample at the BS. Our analysis and computer simulations assume either unit-gain Rayleigh or Rician fading models.

[1]Assuming equiprobable U_2 bits, over a long sequence, half of its samples will have $\sigma_{2,l}^2$ variance while the other half having $\sigma_{2,h}^2$. As a result, the second moment of U_2 samples converges to P.

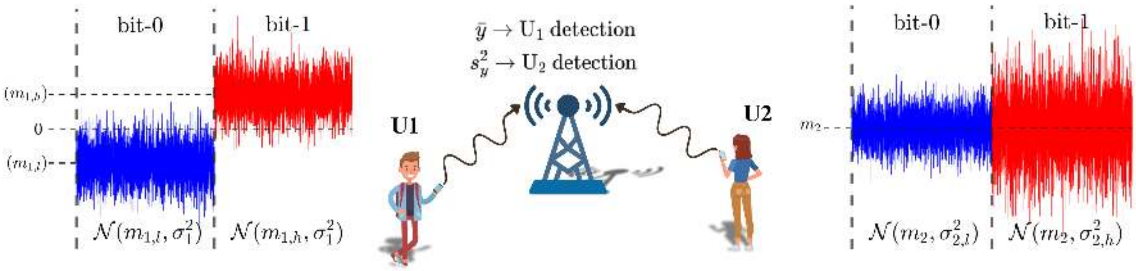

Figure 4.3: Uplink ND-NOMA scheme with two users using real Gaussian signals.

Accordingly, for Rayleigh fading, we have $h_1, h_2 \sim \mathcal{CN}(0,1)$ while for Rician fading with K parameter, we have $h_{1,R}, h_{1,I}, h_{2,R}, h_{2,I} \sim \mathcal{N}\left(\sqrt{\frac{K}{2(1+K)}}, \frac{1}{2(1+K)}\right)$. Then, conditioned on channel coefficients, we obtain

$$\begin{aligned} \mathrm{E}[y^n] =& h_1 m_{1,i} \\ \mathrm{VAR}[y^n] =& |h_1|^2\sigma_1^2 + |h_2|^2\sigma_{2,k}^2 + \sigma_w^2, \quad i,k \in \{l,h\}. \end{aligned} \tag{4.2}$$

The task of the BS is to process the received samples of (4.1) through statistical tests to detect the information bits of both users. The following two subsections present minimum distance-based detection rules for both users and derive their theoretical BEP performance.

4.1.2 Uplink - User 1 Detection

The task of the BS during the detection of U$_1$'s bit involves calculating the sample mean of the received samples, y^n, $n = 1, \ldots, N$, followed by a decision process. In light of this, the sample mean is calculated as

$$\bar{y} = \frac{1}{N}\sum_{n=1}^{N} y^n, \tag{4.3}$$

which is complex Gaussian distributed with mean $\mathrm{E}[\bar{y}] = h_1 m_{1,i}$ (unbiased estimate) and $\mathrm{VAR}[\bar{y}] = (|h_1|^2\sigma_1^2 + |h_2|^2\sigma_{2,k}^2 + \sigma_w^2)/N$ variance with $i,k \in \{l,h\}$. Based on this, the following binary hypothesis test is considered at the BS to detect U$_1$'s bit:

$$\hat{b}_1 = \begin{cases} 0, & \text{if} \quad |\bar{y} - h_1 m_{1,l}|^2 < |\bar{y} - h_1 m_{1,h}|^2 \\ 1, & \text{if} \quad |\bar{y} - h_1 m_{1,h}|^2 < |\bar{y} - h_1 m_{1,l}|^2 . \end{cases} \tag{4.4}$$

The above detector is a "minimum distance detector" and considering the complex Gaussian distribution of $\bar{y}$, it is a *maximum likelihood* one. In light of this and also considering the symmetry for bit-0 and bit-1, conditioned on channel coefficients, the BEP of U_1 becomes

$$P_b = P\left(|\bar{y} - h_1 m_{1,h}|^2 < |\bar{y} - h_1 m_{1,l}|^2 \middle| \, b_1 = 0 \right). \tag{4.5}$$

Expanding the terms in (4.5) and considering $m_{1,h} = -m_{1,l}$, we obtain

$$P_b = P\left(4\mathrm{Re}\left\{\bar{y}h_1^* m_{1,l}\right\} < 0 \,|\, b_1 = 0\right). \tag{4.6}$$

Defining the Gaussian distributed random variable $D = \mathrm{Re}\left\{\bar{y}h_1^* m_{1,l}\right\}$, we obtain, $P_b = P(D < 0 \,|\, b_1 = 0) = Q\left(m_D/\sigma_D\right)$, where $\mathrm{E}[D] = m_D$ and $\mathrm{VAR}[D] = \sigma_D^2$ are conditional statistics of D. While m_D can be easily obtained as $m_D = |h_1|^2 m_{1,l}^2$, derivation of σ_D^2 is not straightforward due to correlation of $\bar{y}_R$ and $\bar{y}_I$. Specifically, we obtain

$$\begin{aligned}
\sigma_D^2 &= \mathrm{VAR}\left[\mathrm{Re}\left\{(\bar{y}_R + j\bar{y}_I)(h_{1,R} + jh_{1,I})m_{1,l}\right\}\right] \\
&= \mathrm{VAR}\left[m_{1,l}\left(\bar{y}_R h_{1,R} + \bar{y}_I h_{1,I}\right)\right] \\
&= m_{1,l}^2 \left(h_{1,R}^2 \mathrm{VAR}\left[\bar{y}_R\right] + h_{1,I}^2 \mathrm{VAR}\left[\bar{y}_I\right]\right. \\
&\qquad\qquad \left. + \, 2h_{1,R}h_{1,I}\mathrm{COV}(\bar{y}_R, \bar{y}_I)\right).
\end{aligned} \tag{4.7}$$

Substituting the following variance values in (4.7) that are obtained after tedious calculations,

$$\begin{aligned}
\mathrm{VAR}\left[\bar{y}_R\right] =& \frac{1}{N}\left(h_{1,R}^2\sigma_1^2 + h_{2,R}^2\sigma_{2,k}^2 + \sigma_w^2/2\right) \\
\mathrm{VAR}\left[\bar{y}_I\right] =& \frac{1}{N}\left(h_{1,I}^2\sigma_1^2 + h_{2,I}^2\sigma_{2,k}^2 + \sigma_w^2/2\right) \\
\mathrm{COV}(\bar{y}_R, \bar{y}_I) =& \frac{1}{N}\left(h_{1,R}h_{1,I}\sigma_1^2 + h_{2,R}h_{2,I}\sigma_{2,k}^2\right),
\end{aligned} \tag{4.8}$$

BEP of U_1 can be obtained as $P_b = Q\left(m_D/\sigma_D\right)$, which is conditioned on h_1, h_2, and $\sigma_{2,k}^2$. Due to the complexity of the terms inside the Q function, we resort to numerical integration methods over the probabilistic distributions of h_1 and h_2 to derive the unconditional BEP. Specifically, we obtain

$$\bar{P}_b = \iiiint P_b f(h_{1,R})f(h_{1,I})f(h_{2,R})f(h_{2,I})dh_{1,R}dh_{1,I}dh_{2,R}dh_{2,I}, \tag{4.9}$$

where a further averaging is needed over the two equiprobable values of $\sigma^2_{2,k}$ for $k \in \{l, h\}$. In order to calculate the unconditional BEP, we encountered a highly complex integral that cannot be solved analytically. Consequently, we utilized numerical methods, specifically Monte Carlo integration, to perform the evaluation. The detailed methodology for this approach is provided in Appendix A and is used to calculate the unconditional BEP among the users on both downlink and uplink scenarios.

Finally, we note that, as NoiseMod schemes, conditional BEP is a decaying function of $\sqrt{N}$ (through σ^2_D).

4.1.3 Uplink - User 2 Detection

In contrast to U_1's mean detection problem, the task of the BS is to formulate a variance detection problem to extract U_2's bits. While we work on a real and positive search space for this problem, complex distributions of y^n and $\bar{y}$, more importantly, their correlated real and imaginary components, pose a severe challenge to the BEP derivation of U_2.

In light of this, the sample variance of the received samples is calculated as

$$s_y^2 = \frac{1}{N-1} \sum_{n=1}^{N} |y^n - \bar{y}|^2 . \tag{4.10}$$

Considering the two possible variance values of y^n, given as $s_0^2 = \sigma_1^2 |h_1|^2 + \sigma_{2,l}^2 |h_2|^2 + \sigma_w^2$ and $s_1^2 = \sigma_1^2 |h_1|^2 + \sigma_{2,h}^2 |h_2|^2 + \sigma_w^2$, further we obtain,

$$\begin{aligned} s_0^2 &= \sigma_w^2 \left(1 + \eta \left|h_1\right|^2 + \delta \left|h_2\right|^2\right) \\ s_1^2 &= \sigma_w^2 \left(1 + \eta \left|h_1\right|^2 + \alpha\delta \left|h_2\right|^2\right) . \end{aligned} \tag{4.11}$$

Here, η, δ, and α are system-related constants defined in Section II.A. Defining a variance threshold as $\gamma = \chi \sigma_w^2$, where χ is the scaled threshold value [Basar, 2024], and it is defined as

$$\chi = \frac{2(1+\delta)(1+\alpha\delta)}{2+\delta(1+\alpha)} . \tag{4.12}$$

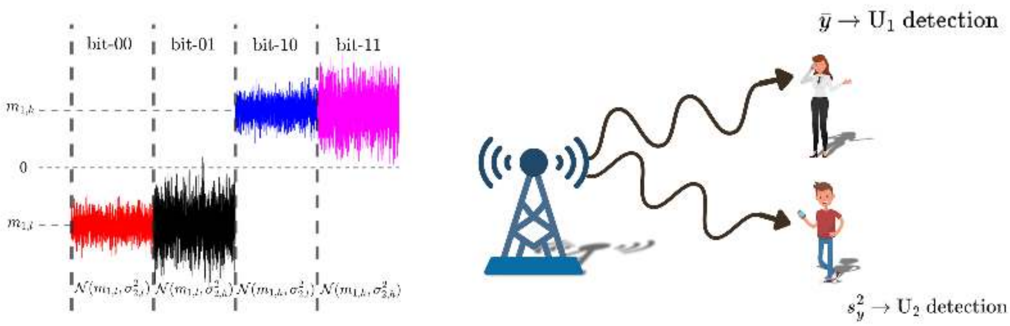

Figure 4.4: Downlink ND-NOMA scheme with two users using real Gaussian signals.

Thus, U$_2$ detection problem is formulated as

$$\hat{b}_2 = \begin{cases} 0, & \text{if} \quad s_y^2 < \gamma \\ 1, & \text{if} \quad s_y^2 > \gamma, \end{cases} \tag{4.13}$$

Accordingly, BEP of U$_2$ bits is obtained as

$$P_b = \frac{1}{2} P\left(s_y^2 > \gamma \middle| b_2 = 0\right) + \frac{1}{2} P\left(s_y^2 < \gamma \middle| b_2 = 1\right). \tag{4.14}$$

This calculation requires the statistics of s_y^2, which will be derived next.

At this point, for large N, to simply the theoretical derivations due to correlated components, we assume $s_y^2 \approx \frac{1}{N-1} \sum_{n=1}^{N} |y^n - h_1 m_{1,i}|^2$, where $\bar{y}$ is replaced by its mean $\mathrm{E}[\bar{y}] = h_1 m_{1,i}$, $i \in \{l, h\}$. Accordingly, (5.12) can be expressed in the quadratic form of $2N$ real Gaussian random variables:

$$\begin{aligned} s_y^2 &= \frac{1}{N-1} \sum_{n=1}^{N} \left(y_R^n - h_{1,R} m_{1,i}\right)^2 + \left(y_I^n - h_{1,I} m_{1,i}\right)^2 \\ &= \mathbf{y}^{\mathrm{T}} \Lambda \mathbf{y}, \end{aligned} \tag{4.15}$$

where $\mathbf{y} \sim \mathcal{N}(\mathbf{0}, \Sigma)$ is a $2N \times 1$ vector with Gaussian distributed elements and Λ is a $2N \times 2N$ diagonal matrix. Here, Σ is a banded covariance matrix, given as

$$\Sigma = \begin{bmatrix} \sigma_R^2 & c & 0 & \dots & & 0 \\ c & \sigma_I^2 & 0 & \dots & & 0 \\ 0 & 0 & \ddots & & & 0 \\ \vdots & \vdots & \dots & 0 & \sigma_R^2 & c \\ 0 & 0 & \dots & 0 & c & \sigma_I^2 \end{bmatrix}_{2N \times 2N} \tag{4.16}$$

where $\sigma_R^2 = \mathrm{VAR}[y_R^n] = h_{1,R}^2\sigma_1^2 + h_{2,R}^2\sigma_{2,k}^2 + \sigma_w^2/2$, $\sigma_I^2 = \mathrm{VAR}[y_I^n] = h_{1,I}^2\sigma_1^2 + h_{2,I}^2\sigma_{2,k}^2 + \sigma_w^2/2$, and $c = \mathrm{COV}((y_R^n - h_{1,R}m_{1,i}), (y_I^n - h_{1,I}m_{1,i}))$ for $i,k \in \{l,h\}$ and $n = 1,\ldots,N$. After simple manipulations, we obtain $c = h_{1,R}h_{1,I}\sigma_1^2 + h_{2,R}h_{2,I}\sigma_{2,k}^2$.

At this point, interested readers might resort to advanced statistics by considering series expansions for the distribution of Gaussian quadratic forms or advanced mathematical packages on generalized chi-square distributions [Mathai and Provost, 1992]. To simplify our analysis, we consider the central limit theorem (CLT) and assume that $s_y^2 \sim \mathcal{N}(\mu_s, \sigma_s^2)$ for large enough N.

From [Paolella, 2018], we obtain the mean and variance of s_y^2 as

$$\begin{aligned}\mu_s &= \frac{1}{N-1}\mathrm{tr}[\Lambda\Sigma] = \frac{N(\sigma_R^2+\sigma_I^2)}{N-1}\\ \sigma_s^2 &= \frac{2}{(N-1)^2}\mathrm{tr}[\Lambda\Sigma\Lambda\Sigma] = \frac{2N}{(N-1)^2}\left(\sigma_R^4+\sigma_I^4+2c^2\right),\end{aligned} \tag{4.17}$$

which are consistent with the definition of s_y^2 in (5.12). Accordingly, BEP is obtained as

$$P_b = \frac{1}{2}Q\left(\frac{\gamma - \mu_{s\,|b_2=0}}{\sigma_{s\,|b_2=0}}\right) + \frac{1}{2}Q\left(\frac{\mu_{s\,|b_2=1} - \gamma}{\sigma_{s\,|b_2=1}}\right) \tag{4.18}$$

where μ_s and σ_s are conditioned on the transmitted bit through $\sigma_{2,k}^2$. Selecting the threshold for equal bit error probabilities of bit 0 and bit 1 yields

$$\gamma = \frac{\sigma_{s\,|b_2=0}\times\mu_{s\,|b_2=1} + \sigma_{s\,|b_2=1}\times\mu_{s\,|b_2=0}}{\sigma_{s\,|b_2=0}+\sigma_{s\,|b_2=1}}. \tag{4.19}$$

Substituting this value in (4.18) yields the conditional BEP as

$$P_b = Q\left(\frac{\mu_{s\,|b_2=1} - \mu_{s\,|b_2=0}}{\sigma_{s\,|b_2=0}+\sigma_{s\,|b_2=1}}\right). \tag{4.20}$$

As U_1's BEP, for $N \gg 1$, we observe that U_2's BEP is a decaying function of $\sqrt{N}$ through the σ_s^2 term in the Q function.

Despite its simple detection architecture and our assumptions above, the final result for the BEP is still too complicated for taking an average over channel realizations, and we have to use numerical integration as in (4.9) to obtain unconditional BEP. Nevertheless, the computational complexity of our approach remains significantly lower than traditional PAM demodulation methods with SIC, which

Table 4.1: Statistics of the transmitted and received signals for Downlink ND-NOMA

U_1/U_2 bits	s_{BS}^n	$y_p^n,\, p \in \{1,2\}$
00	$\mathcal{N}(m_{1,l}, \sigma_{2,l}^2)$	$\mathcal{CN}(h_p m_{1,l}, \|h_p\|^2 \sigma_{2,l}^2 + \sigma_w^2)$
01	$\mathcal{N}(m_{1,l}, \sigma_{2,h}^2)$	$\mathcal{CN}(h_p m_{1,l}, \|h_p\|^2 \sigma_{2,h}^2 + \sigma_w^2)$
10	$\mathcal{N}(m_{1,h}, \sigma_{2,l}^2)$	$\mathcal{CN}(h_p m_{1,h}, \|h_p\|^2 \sigma_{2,l}^2 + \sigma_w^2)$
11	$\mathcal{N}(m_{1,h}, \sigma_{2,h}^2)$	$\mathcal{CN}(h_p m_{1,h}, \|h_p\|^2 \sigma_{2,h}^2 + \sigma_w^2)$

require iterative interference cancellation and complex computations. In contrast, our detection methods rely solely on straightforward mean, variance, and threshold calculations, making them far more efficient and less computationally demanding.

The following steps outline the key aspects of the uplink system model, summarizing the transmission and detection processes:

- *Step 1*: U_1 encodes bits by adjusting the mean of its Gaussian noise signal (low for bit-0, high for bit-1), while U_2 encodes bits by varying the variance (low for bit-0, high for bit-1) with its mean kept at zero to avoid interference.

- *Step 2*: The base station receives the combined signals from U_1 and U_2, affected by channel fading and noise.

- *Step 3*: The base station decodes U_1's bit by computing the mean of received samples and uses a minimum distance detector, while U_2's bit is decoded by computing the variance and applying a threshold-based detector.

4.2 Downlink ND-NOMA: System Model and Performance Analysis

In this section, we emphasize downlink ND-NOMA for two users by defining its system model and then presenting its theoretical BEP performance.

4.2.1 System Model

As shown in Fig. 4.4, for the downlink scheme, a composite signal is generated by the BS considering the information bits of two users. Here, we again consider binary modulation for simplicity. Accordingly, BS's transmitted noise samples follow $s_{BS}^n \sim \mathcal{N}(m_{1,i}, \sigma_{2,k}^2)$ distribution for $i, k \in \{l, h\}$. In other words, the mean of the transmitted signal is dictated by U_1's bit while its variance is determined according to U_2's bit. In this case, the received signals at two users are given by

$$\begin{aligned} y_1^n &= h_1 s_{BS}^n + w_1^n \\ y_2^n &= h_2 s_{BS}^n + w_2^n, \end{aligned} \tag{4.21}$$

for $n = 1, \ldots, N$. Here, h_1 and h_2 stand for the downlink channel fading coefficients between the BS and users, and w_1^n and w_2^n are AWGN samples at users with $\mathcal{CN}(0, \sigma_w^2)$ distribution. Specifically, Table I lists the distribution of the transmitted and received signals at all terminals depending on four user bit combinations, $00, 01, 10$, and 11, where the first and second bits respectively stand for U_1 and U_2 bits for a given bit duration.

Here, we assume that the total transmission power is fixed to P, that is, $E[(s_{BS}^n)^2] = P$. Similar to the β parameter of the uplink scheme, we define a new parameter, ψ, as the portion of U_1's allocated power, that is, $m_{1,l}^2 = m_{1,h}^2 = \psi P$ (dc power of the transmitted signal). Accordingly, for U_2, we have $(\sigma_{2,l}^2 + \sigma_{2,h}^2)/2 = (1 - \psi)P$ (ac power of the transmitted signal). We again consider $m_{1,h} = -m_{1,l}$ and $\sigma_{2,h}^2 = \alpha \sigma_{2,l}^2$.

Since the users' signals do not overlap as in the uplink scheme, the detection model of the downlink system is much simpler, and there is no interaction among user signals. Furthermore, there is no need for successive interference cancellation and error propagation issues as in the downlink PD-NOMA scheme. In what follows, we provide detector architectures for both users.

4.2.2 Downlink - User 1 Detection

The receiver architecture of the downlink scheme for U_1 is very similar to that of the uplink scheme, and the BEP can be evaluated by simple modifications. Specifically, U_1 calculates the sample mean of its received samples as $\bar{y}_1 = \frac{1}{N}\sum_{n=1}^{N} y_1^n$, which is also Gaussian distributed with $\mathrm{E}[\bar{y}_1] = h_1 m_{1,i}$ and $\mathrm{VAR}[\bar{y}_1] = (|h_1|^2 \sigma_{2,k}^2 + \sigma_w^2)/N$ for

$i, k \in \{l, h\}$. Accordingly, the minimum distance detector is formulated as

$$\hat{b}_1 = \begin{cases} 0, & \text{if} \quad |\bar{y}_1 - h_1 m_{1,l}|^2 < |\bar{y}_1 - h_1 m_{1,h}|^2 \\ 1, & \text{if} \quad |\bar{y}_1 - h_1 m_{1,h}|^2 < |\bar{y}_1 - h_1 m_{1,l}|^2 . \end{cases} \tag{4.22}$$

Similar to the uplink scheme's BEP in (4.5), BEP for this case is obtained as

$$\begin{aligned} P_b &= P\left(|\bar{y}_1 - h_1 m_{1,h}|^2 < |\bar{y}_1 - h_1 m_{1,l}|^2 \,\middle|\, b_1 = 0\right). \\ &= P\left(\mathrm{Re}\left\{\bar{y}_1 h_1^* m_{1,l}\right\} < 0 \mid b_1 = 0\right) \\ &= P(D < 0 \mid b_1 = 0) = Q\left(m_D/\sigma_D\right). \end{aligned} \tag{4.23}$$

Here, Gaussian distributed variable D has the following statistics: $m_D = |h_1|^2 m_{1,l}^2$ and $\sigma_D^2 = m_{1,l}^2(h_{1,R}^2 \mathrm{VAR}\left[\bar{y}_{1,R}\right] + h_{1,I}^2 \mathrm{VAR}\left[\bar{y}_{1,I}\right] + 2h_{1,R}h_{1,I}\mathrm{COV}(\bar{y}_{1,R}, \bar{y}_{1,I}))$. With simple manipulations, variance values are obtained as

$$\begin{aligned} \mathrm{VAR}\left[\bar{y}_{1,R}\right] =& \frac{1}{N}\left(h_{1,R}^2 \sigma_{2,k}^2 + \sigma_w^2/2\right) \\ \mathrm{VAR}\left[\bar{y}_{1,I}\right] =& \frac{1}{N}\left(h_{1,I}^2 \sigma_{2,k}^2 + \sigma_w^2/2\right) \\ \mathrm{COV}(\bar{y}_{1,R}, \bar{y}_{1,I}) =& \frac{1}{N} h_{1,R} h_{1,I} \sigma_{2,k}^2. \end{aligned} \tag{4.24}$$

Conditional BEP is obtained by substituting these values in σ_D^2 first and then considering (4.23).

4.2.3 Downlink - User 2 Detection

Finally, this subsection investigates the receiver architecture and performance of U_2 for the downlink scheme. Fortunately, the same analytical framework of Section II.C can be considered here for slight modifications.

For U_2's variance detection in the downlink scheme, the sample variance is obtained as

$$s_{y_2}^2 = \frac{1}{N-1} \sum_{n=1}^{N} |y_2^n - \bar{y}_2|^2 \tag{4.25}$$

where $\bar{y}_2$ is the sample mean for the samples of U_2. Here, in a similar manner to uplink detection, we define a variance threshold as $\gamma = \chi \sigma_w^2$ and formulate the U_2

detection problem as

$$\hat{b}_2 = \begin{cases} 0, & \text{if} \quad s_{y_2}^2 < \gamma \\ 1, & \text{if} \quad s_{y_2}^2 > \gamma. \end{cases} \tag{4.26}$$

In light of this, BEP of the U_2 bit is obtained as

$$P_b = \frac{1}{2} P\left(s_{y_2}^2 > \gamma \middle| b_2 = 0\right) + \frac{1}{2} P\left(s_{y_2}^2 < \gamma \middle| b_2 = 1\right). \tag{4.27}$$

To use the same analysis of Section III.C, we again resort to the strong law of large numbers by assuming $s_{y_2}^2 \approx \frac{1}{N-1} \sum_{n=1}^{N} |y_2^n - h_2 m_{1,i}|^2$. Expressing, this new $s_{y_2}^2$ in the quadratic form of $2N$ real Gaussian random variables as $s_{y_2}^2 = \mathbf{y}^{\mathrm{T}} \Lambda \mathbf{y}$, where $\mathbf{y}$ and Λ are as defined in (4.15), we obtain the same banded covariance matrix of (4.16) with the following updated parameters:

$$\begin{aligned} \sigma_R^2 &= \mathrm{VAR}[y_{2,R}^n] = h_{2,R}^2 \sigma_{2,k}^2 + \sigma_w^2/2 \\ \sigma_I^2 &= \mathrm{VAR}[y_{2,I}^n] = h_{2,I}^2 \sigma_{2,k}^2 + \sigma_w^2/2 \\ c &= \mathrm{COV}\big(\left(y_{2,R}^n - h_{2,R} m_{1,i}\right), \left(y_{2,I}^n - h_{2,I} m_{1,i}\right)\big) \\ &= h_{2,R} h_{2,I} \sigma_{2,k}^2. \end{aligned} \tag{4.28}$$

Considering CLT and substituting the new values of (4.28) first in (4.17), then updating (4.18)-(4.20) accordingly, conditional BEP is obtained.

As mentioned in the uplink scheme, the detection methods employed maintain the same computational complexity, avoiding the intensive iterative interference cancellation and numerical computations required in traditional PAM demodulation with SIC.

The following steps outline the key aspects of the downlink system model, summarizing the transmission and detection processes:

- *Step 1*: The BS transmits a Gaussian noise signal where the mean and variance encode U_1's and U_2's bits, respectively.

- *Step 2*: U_1 estimates its bit by computing the mean of received samples using a minimum distance detector.

Table 4.2: Simulation Parameters

Parameter	**Value**
K_{dB}	5, 10
N	50, 100
δ_{dB}	[-40, 5]
α	10
P_{dBm}	30
β	1/100

- *Step 3*: U_2 estimates its bit by computing the variance of received samples using a threshold-based detector.

4.3 Numerical Results

In this section, we analyze the bit error rate BER performance of the proposed ND-NOMA system in both uplink and downlink scenarios. In our analysis, the channel coefficients are modeled as if their envelopes are Rician distributed, $h_{1,R}, h_{1,I}, h_{2,R}, h_{2,I} \sim \mathcal{N}\left(\sqrt{\frac{K}{2(1+K)}}, \frac{1}{2(1+K)}\right)$, where K being the Rician factor. This choice of distribution reflects the presence of a line-of-sight component along with multipath effects, capturing the realistic propagation conditions for the wireless channels considered in our study. Moreover, we employed the Monte Carlo integration method, as described in Appendix A, to compute the unconditional BEP for uplink and downlink scenarios so as to verify our computer simulation results. The simulation parameters are outlined in Table II.

4.3.1 Uplink Scenario

Figs. 4.5(a) and 4.5(b) illustrate the BER performance of U_1 and U_2 for $K \in \{5, 10\}$ respectively where our theoretical derivations verify our simulation results. Herein, the increase in the Rician K-factor improves the BER performance of the proposed

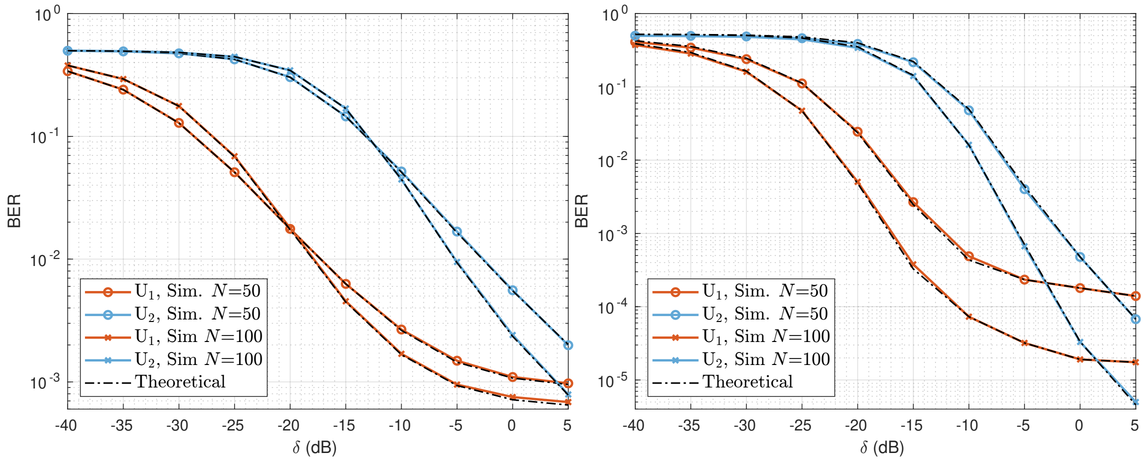

(a) (b)

Figure 4.5: Theoretical BEP and simulated BER for uplink ND-NOMA versus $\delta = \sigma_{2,l}^2/\sigma_w^2$, with Rician K-factor values of (a) $K = 5$ and (b) $K = 10$ dB

ND-NOMA system. This enhancement is attributed to the stronger line-of-sight component in the Rician channel, which enhances detection performance for both U_1 and U_2 in the uplink scenario. In Fig. 4.5(b) where $K = 10$, U_1 exhibits better BER performance compared to U_2, since U_1's detection mechanism leverages the mean of the transmitted Gaussian samples, which is more resilient to noise variations compared to U_2's variance-based detection in our scenario.

The impact of δ on BER is also critical in the uplink scenario. In Figs. 4.5 and 4.6, increasing δ, which represents the higher ratio of useful to disruptive noise variances, results in improved BER performance as depicted in Figs. 4.5(a) and 4.5(b). However, in Fig.4.5 (b), after the δ value of -5, BER saturates where $N = 50$ for U_1, since there is an interference between the users. This trend is evident in Figs. 4.5(a) and 4.5(b), where higher δ values correlate with improved BER performance. The ability of ND-NOMA to maintain low BER even in scenarios with significant noise variance is demonstrated, indicating its effectiveness in environments with varying noise conditions. It is worth noting that the users of ND-NOMA are not interference-free; nevertheless, its unique nature allows the BS to distinguish user signals without SIC.

Furthermore, another important parameter that significantly affects the BER

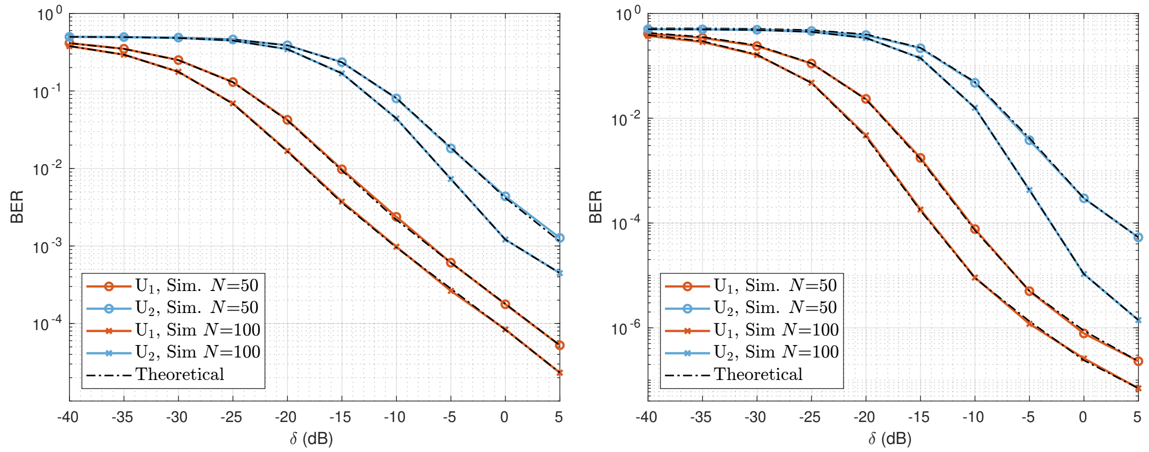

(a) (b)

Figure 4.6: Theoretical BEP and simulated BER for downlink ND-NOMA versus $\delta = \sigma^2_{2,l}/\sigma^2_w$, with Rician K-factor values of (a) $K = 5$ and (b) $K = 10$ dB

performance of the proposed ND-NOMA system is the number of noise samples per bit (N), which stands for the number of samples that are taken to estimate the mean for U_1 and estimate the variance for U_2. As can be seen in Figs. 4.5 (a) and 4.5 (b), increasing N boosts the performance of the system's uplink scenario. Our findings also underscore the importance of sample size N in reducing BER, highlighting that the transition from N being 50 to 100 sample size allows better estimation accuracy of the Gaussian noise parameters, thus minimizing the impact of noise as well as improving overall detection performance.

4.3.2 Downlink Scenario

As in the uplink scenario, the downlink scenario's simulation results coincide with our theoretical derivations, in Figs. 4.6(a) and 4.6(b), demonstrating the system's reliability even in the highly disruptive noise conditions. As expected, the increase in δ as well as K enhances the BER performance of the proposed system in the downlink scenario for U_1 and U_2. Increasing δ as well as N and K improves the system performance. Different from the uplink scenario where $K = 10$, the BER performance of the ND-NOMA system of U_1 does not saturate after a specific δ value since there is no interference.

We note that the impact of the sample size N on the BER in the downlink

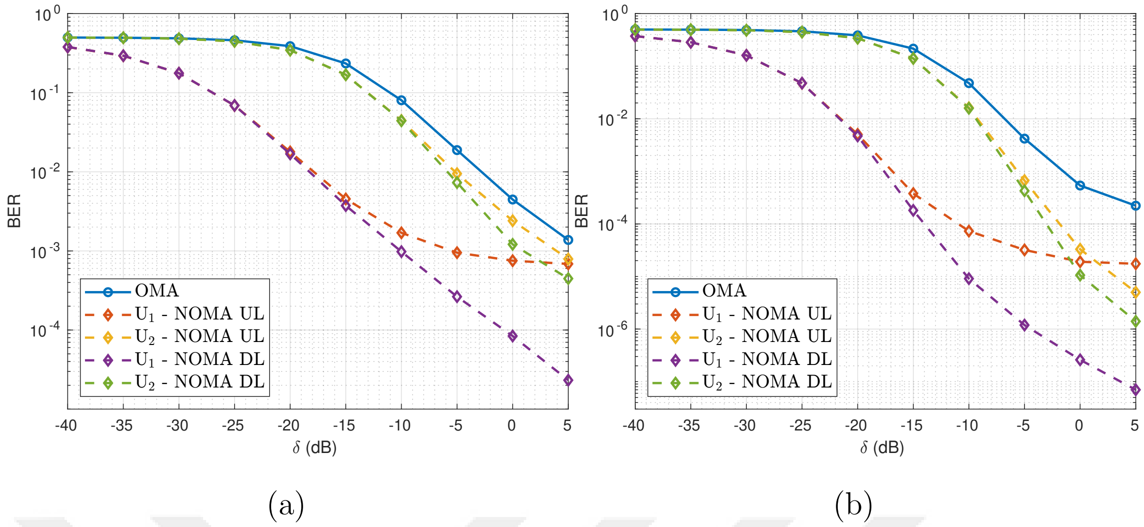

Figure 4.7: Comparative BER performance of OMA-NoiseMod and ND-NOMA (uplink and downlink) with respect to δ, with Rician K-factor values of (a) $K = 5$ and (b) $K = 10$ dB

scenario is significant. As N increases, the BER decreases for both U_1 and U_2. This is due to the fact that larger sample sizes allow for better averaging of the noise parameters, which are supported by a minimum distance detector for mean detection at U_1 and a threshold-based detector for variance detection at U_2, which improves the accuracy of related parameters. Consequently, the ND-NOMA system achieves lower BER with higher N, demonstrating its efficiency and reliability in maintaining high-quality communication in downlink scenarios.

Comparing Fig. 4.5(b) with Fig. 4.6(b), where uplink and downlink scenarios are considered respectively, the BER performance of U_2 exhibits similar results for both scenarios. However, two bits are transmitted in the downlink scenario, unlike the uplink scenario, where one bit of information is conveyed at every transmission instant. Furthermore, U_1 BER gets saturated since there is an interference in the uplink scenario; however, in the downlink scenario, since we assume that U_1 signal does not interfere with U_2 signal, its performance does not reach saturation. Additionally, we have presented the OMA-NoiseMod scenario in the following subsection to prevent interference between users.

4.3.3 Comparison with OMA-NoiseMod Scenario

In scenarios where two users communicate simultaneously over N noise samples in uplink/downlink, the communication can be divided into two equal parts, $N/2$ - $N/2$, allowing classic NoiseMod communication without interference. This scheme can be referred to as OMA-NoiseMod. For the evaluation of the BER of ND-NOMA under comparable modulation principles, we introduce OMA-NoiseMod as a benchmark. Unlike conventional OMA schemes employing standard amplitude and phase modulations, OMA-NoiseMod enables a fairer comparison by operating under similar noise-domain constraints. While traditional OMA inherently avoids multi-user interference and thus achieves superior BER, such a comparison would not be meaningful given the fundamentally different transmission mechanisms of traditional amplitude/phase modulation and NoiseMod schemes. It would not be a fair comparison to compare ND-NOMA schemes with the traditional (for instance, phase shift keying-based) NOMA schemes since δ dictates the ratio between useful and disruptive noise variances, its effect on detection performance is fundamentally different.

Figs. 4.7(a) and 4.7(b) illustrate the comparative BER performance of ND-NOMA and the OMA-NoiseMod scenario for both uplink and downlink transmissions. As shown in Fig. 4.7(a), ND-NOMA outperforms OMA-NoiseMod in terms of BER under the same conditions, particularly as the Rician K-factor and δ increase.

In the higher Rician K-factor scenario ($K = 10$), as shown in Fig. 4.7(b), ND-NOMA continues to exhibit superior BER performance compared to OMA-NoiseMod. The key advantage of ND-NOMA over OMA-NoiseMod lies in its ability to manage user interference through the simultaneous transmission of data. The results clearly show that with an increased number of noise samples (N) and higher Rician K-factors, ND-NOMA achieves lower BER compared to OMA-NoiseMod. This makes ND-NOMA a more efficient and reliable communication scheme.

In the OMA-NoiseMod scenario, both U_1 and U_2 experience the same BER performance because the communication process is divided into non-overlapping time slots or frequency bands, ensuring that both users have identical conditions for transmitting and receiving data. This means there is no interference between the users, and both experience the same signal quality and noise conditions, leading to identical BER outcomes. This explains the reason why their performances are the same in the OMA-NoiseMod scheme.

Chapter 5

THREE USER NOISE-DOMAIN NON-ORTHOGONAL MULTIPLE ACCESS

In this chapter, we propose a novel ND-NOMA framework that enables simultaneous communication among three users by utilizing independent statistical properties of the Gaussian noise: mean, variance, and correlation. In this setup, the first user embeds information into the mean of the noise samples, the second user manipulates the variance, and the third user cleverly modulates the correlation between consecutive noise samples to convey data. We present system models for both uplink and downlink scenarios and develop dedicated detection mechanisms customized to each user's encoding strategy. Simulation results and theoretical analysis are provided under Rician fading channels to evaluate BER performance. The numerical results confirm that our proposed scheme retains the low BER and low-complexity characteristics over Rician fading channels, while significantly enhancing multi-user support. Hence, our proposed scheme specifically reduces the system complexity, which enables suitability for Internet-of-Things (IoT) environments. In order to support reliable multi-user communication under the power constraints of future IoT cities, the three-user ND-NOMA system uses a diverse detection architecture: mean-based detection for the first user, variance thresholding for the second user, and correlation detection for the third user. This layered detection structure of the three-uesr ND-NOMA significantly enhances robustness, maintaining reliability even under challenging channel conditions, while entirely eliminating the need for SIC thanks to its orthogonal modulation over mean, variance, and correlation.

The rest of the chapter is organized as follows. Section 5.1 presents the system model and detection rules for the uplink scenario. Section 5.2 extends the analysis to the downlink case. Section 5.3 provides simulation results and performance

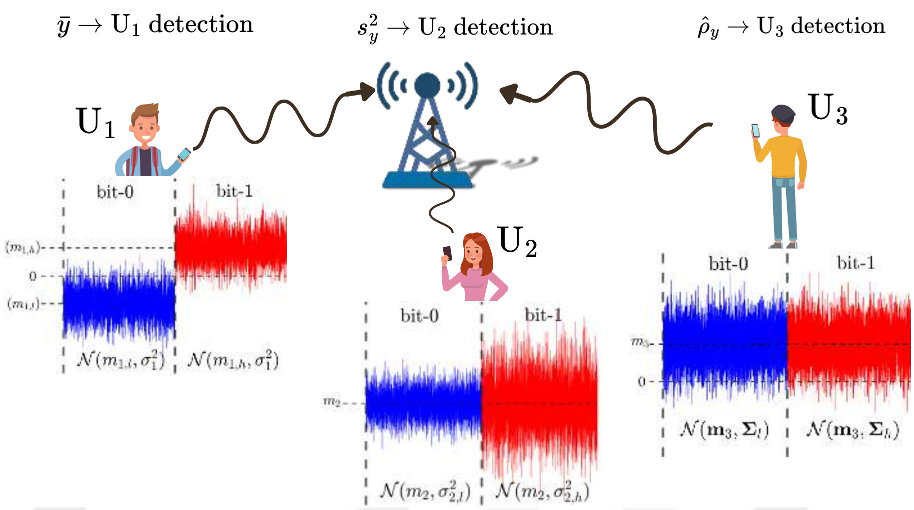

Figure 5.1: Uplink ND-NOMA scheme with three users using real Gaussian signals.

discussions.

5.1 Uplink ND-NOMA for Three Users: System Model and Performance Analysis

In this section, we introduce the ND-NOMA for three users scheme. In the proposed scheme, each user utilizes a distinct noise-domain property to encode data: mean, variance, and correlation. Building on the two-user ND-NOMA framework, we propose a new model by introducing a third user whose information is embedded in the correlation between pairs of Gaussian noise samples. We also provide a general framework to evaluate the uplink BER performance for all users under Rician fading channel scenarios.

5.1.1 System Model

As illustrated in Fig. 5.1, the uplink transmission of the ND-NOMA for three users system encodes the information through the distinct statistical features of the Gaussian noise. To be specific, User 1 (U$_1$) modulates the mean, User 2 (U$_2$) modulates the variance, and User 3 (U$_3$) modulates the correlation between the Gaussian samples. In our new scheme, each user transmits its bit using N real Gaussian noise samples per bit period.

For U_1, information bits are transmitted by altering the mean of Gaussian samples, while keeping the variance constant. That is, for bit-0 and bit-1, we have $s_1^n \sim \mathcal{N}(m_{1,l}, \sigma_1^2)$ and $s_1^n \sim \mathcal{N}(m_{1,h}, \sigma_1^2)$, with fixed variance σ_1^2 and means $m_{1,h} = -m_{1,l}$ assumed for symmetry and optimal detection. Each s_1^n is real-valued and independently generated.

U_2 follows a variance modulation scheme, transmitting zero-mean Gaussian samples with two possible variances depending on the bit. That is, for bit-0 and bit-1, we have $s_2^n \sim \mathcal{N}(0, \sigma_{2,l}^2)$ and $s_2^n \sim \mathcal{N}(0, \sigma_{2,h}^2)$, with fixed mean 0 and variances satisfying $\sigma_{2,h}^2 = \alpha\sigma_{2,l}^2$, where $\alpha > 1$. Here, α represents the ratio between the high and low variance levels used by U_2. Unlike phase and frequency modulations, variance modulation encodes information in the power level of noise rather than its shape or position.

U_3 modulates the correlation structure between pairs of noise samples to encode its bits. Each bit period consists of N real samples grouped into $N/2$ correlated pairs. The samples are jointly Gaussian with a non-zero mean vector $\mathbf{m}_3 = [m_3,\ m_3]^\top$ and a covariance matrix determined by the information bit:

$$\mathbf{s}_3^n \sim \mathcal{N}(\mathbf{m}_3, \mathbf{\Sigma}_k), \quad \mathbf{\Sigma}_k = \sigma_3^2 \begin{bmatrix} 1 & \rho_k \\ \rho_k & 1 \end{bmatrix}, \quad k \in \{l, h\}$$

where ρ_l and ρ_h correspond to bit-0 and bit-1, respectively. Here, b_1, b_2, and b_3 represent the information bits of U_1, U_2, and U_3, respectively. Specifically, b_1 is conveyed by modulating the mean of the Gaussian noise samples, b_2 by modulating the variance, and b_3 by modulating the correlation coefficient between two jointly Gaussian noise samples.

We assume an average transmit power of P for each user, which corresponds to the second moment of the transmitted samples. For U_1, this leads to $P = m_{1,l}^2 + \sigma_1^2$. A power allocation parameter $\beta \in (0, 1)$ is defined such that $\sigma_1^2 = \beta P$ and $m_{1,l}^2 = (1-\beta)P$. For U_2, assuming equiprobable bits, the average power is given by $P = (\sigma_{2,l}^2 + \sigma_{2,h}^2)/2$. For U_3, the power constraint is satisfied by keeping the marginal variances fixed at σ_3^2, such that each individual sample still satisfies $\mathbb{E}[(s_3^n)^2] = P$.

To facilitate the analysis, we define $\delta = \sigma_{2,l}^2/\sigma_w^2$ as the normalized low-variance parameter of U_2, and $\alpha = \sigma_{2,h}^2/\sigma_{2,l}^2$ as the high-to-low variance ratio. Additionally, the normalized variance of U_1 becomes $\eta = \sigma_1^2/\sigma_w^2 = \frac{(1+\alpha)\delta\beta}{2}$.

The nth received sample at the base station is expressed as

$$y^n = h_1 s_1^n + h_2 s_2^n + h_3 s_3^n + w^n, \quad n = 1, \ldots, N, \tag{5.1}$$

where h_1, h_2, and h_3 denote the complex baseband fading coefficients between U_1, U_2, U_3 and the base station, respectively, and $w^n \sim \mathcal{CN}(0, \sigma_w^2)$ represents the additive white Gaussian noise (AWGN). We assume that our channel conditions are under the effects of Rician fading. Under Rician fading with factor K, we have:

$$h_{i,R},\ h_{i,I} \sim \mathcal{N}\left(\sqrt{\frac{K}{2(1+K)}}, \frac{1}{2(1+K)}\right), \quad i = 1, 2, 3. \tag{5.2}$$

where R and I correspond to the real and imaginary components of the complex channel coefficient h_i, respectively, and i denotes the user index in the system.

Conditioned on the transmitted bits and channel coefficients, the received signal has the following mean and variance:

$$\begin{aligned} \mathrm{E}[y^n] &= h_1 m_{1,i} + h_3 m_3, \\ \mathrm{VAR}[y^n] &= |h_1|^2\sigma_1^2 + |h_2|^2\sigma_{2,k}^2 + |h_3|^2\sigma_3^2 + \sigma_w^2, \end{aligned} \tag{5.3}$$

where $i, k \in \{l, h\}$ refer to the mean and variance bit indices of U_1 and U_2, respectively.

The base station (BS) jointly receives all users' signals over different channels and must extract each bit via statistical inference on the received samples. The next sections present the detection strategies and theoretical bit error probability (BEP) derivations for all three users.

5.1.2 Uplink – User 1 Detection

In the ND-NOMA for three users uplink system, the BS detects U_1's bit by leveraging the fact that U_1 uses mean modulation. That is, each bit is transmitted over N independent real Gaussian samples whose mean alternates depending on the bit value, while the variance remains fixed. To retrieve this embedded information, the BS computes the empirical mean of the received signal across the N samples:

$$\bar{y} = \frac{1}{N}\sum_{n=1}^{N} y^n, \tag{5.4}$$

where y^n denotes the received signal at time index n. Due to the presence of multiple users and additive noise, $\bar{y}$ is a complex-valued random variable following a Gaussian distribution whose mean and variance are influenced by all three users' transmission parameters and the instantaneous channel realizations.

Specifically, the conditional mean of $\bar{y}$, given the channel coefficients and transmitted bits, is expressed as $\mathbb{E}[\bar{y}] = h_1 m_{1,i} + h_3 m_3$, where $m_{1,i}$ represents the bit-dependent mean value transmitted by U_1 and m_3 is the constant mean of the samples transmitted by U_3. Here, h_1 and h_3 denote the complex baseband fading coefficients between the BS and U_1 and U_3, respectively. The term $h_1 m_{1,i}$ reflects the desired signal component, while $h_3 m_3$ acts as structured interference due to the non-zero mean of U_3's signal.

The variance of $\bar{y}$, conditioned on the transmitted bits, is given by

$$\mathrm{VAR}[\bar{y}] = \frac{1}{N}\left(|h_1|^2\sigma_1^2 + |h_2|^2\sigma_{2,k}^2 + \eta P|h_3|^2 + \sigma_w^2\right), \tag{5.5}$$

where σ_1^2 is the fixed variance used by U_1, and $\sigma_{2,k}^2$ is the bit-dependent variance of the zero-mean samples sent by U_2, with $k \in \{l, h\}$ indicating low or high variance depending on the bit. The parameter ηP represents the average power allocated to U_3's correlation-modulated signal, which contributes additional variability to the received signal. Finally, σ_w^2 is the variance of the AWGN at the BS.

Given this statistical structure, the BS applies a minimum-distance decision rule to determine U_1's transmitted bit. The detector compares the received mean to two hypotheses, each corresponding to one of the possible transmitted means:

$$\hat{b}_1 = \begin{cases} 0, \text{if } |\bar{y} - h_1 m_{1,l} - h_3 m_3|^2 < |\bar{y} - h_1 m_{1,h} - h_3 m_3|^2, \\ 1, \text{if } |\bar{y} - h_1 m_{1,h} - h_3 m_3|^2 < |\bar{y} - h_1 m_{1,l} - h_3 m_3|^2. \end{cases} \tag{5.6}$$

This rule corresponds to a minimum distance detector applied in the mean domain. The detector compares the sample mean of the received signal with two predefined reference means, each representing one of the two possible transmitted symbols. These reference means incorporate the average power contributions from the other two users, making the detector resilient to their interference without requiring explicit cancellation.

Under the assumption of symmetry between bit-0 and bit-1, and without loss of generality, we consider the probability of error when bit-0 is transmitted. Letting $m_{1,h} = -m_{1,l}$ for analytical simplicity, the conditional BEP becomes

$$P_b = P\Big(|\bar{y} - h_1 m_{1,h} - h_3 m_3|^2 < |\bar{y} - h_1 m_{1,l} - h_3 m_3|^2 \mid b_1 = 0\Big). \tag{5.7}$$

This expression is further simplified by defining a decision variable $D = \mathrm{Re}\{(\bar{y} - h_3 m_3) h_1^* m_{1,l}\}$, which is a real-valued Gaussian random variable with mean $m_D = \mathbb{E}[D] = |h_1|^2 m_{1,l}^2$ and variance $\mathrm{VAR}[D] = \sigma_D^2$. The BEP is thus rewritten in Q-function form as

$$P_b = Q\left(\frac{m_D}{\sigma_D}\right) \tag{5.8}$$

where the variance σ_D^2 captures the uncertainty in the detection variable and is given by

$$\sigma_D^2 = m_{1,l}^2 \left(h_{1,R}^2 \mathrm{VAR}[\bar{y}_R] + h_{1,I}^2 \mathrm{VAR}[\bar{y}_I] + 2 h_{1,R} h_{1,I} \mathrm{COV}(\bar{y}_R, \bar{y}_I)\right) \tag{5.9}$$

$\bar{y}_R$, $\bar{y}_I$ being the corresponding components of $\bar{y}$. The individual variances and covariances in this expression are computed as follows:

$$\begin{aligned}
\mathrm{VAR}[\bar{y}_R] &= \frac{1}{N}\left(h_{1,R}^2 \sigma_1^2 + h_{2,R}^2 \sigma_{2,k}^2 + \eta P h_{3,R}^2 + \frac{\sigma_w^2}{2}\right), \\
\mathrm{VAR}[\bar{y}_I] &= \frac{1}{N}\left(h_{1,I}^2 \sigma_1^2 + h_{2,I}^2 \sigma_{2,k}^2 + \eta P h_{3,I}^2 + \frac{\sigma_w^2}{2}\right), \\
\mathrm{COV}(\bar{y}_R, \bar{y}_I) &= \frac{1}{N}\Big(h_{1,R} h_{1,I} \sigma_1^2 + h_{2,R} h_{2,I} \sigma_{2,k}^2 + \eta P h_{3,R} h_{3,I}\Big)
\end{aligned} \tag{5.10}$$

Since this BEP expression depends on the random fading coefficients h_1, h_2, h_3, and the bit-dependent variance $\sigma_{2,k}^2$, we average over all distributions to obtain the unconditional BEP. Respectively, we obtain

$$\begin{aligned}
\bar{P}_b = \int\!\!\int\!\!\int\!\!\int\!\!\int\!\!\int P_b \cdot f(h_{1,R}) f(h_{1,I}) f(h_{2,R}) f(h_{2,I}) f(h_{3,R}) f(h_{3,I})\, dh_{1,R}\, dh_{1,I}\, dh_{2,R}\, dh_{2,I} \\
\cdot\, dh_{3,R}\, dh_{3,I},
\end{aligned} \tag{5.11}$$

where averaging is also performed over the two equiprobable values of $\sigma^2_{2,k}$. Since this integral is analytically intractable due to the complex dependencies within the Q function, we employ Monte Carlo integration method, as detailed in Appendix A, to numerically estimate the unconditional BEP.

5.1.3 Uplink – User 2 Detection

Unlike the U_1's mean detection scheme, this time BS involves a variance-based detection process in order to detect the bit of U_2. In this detection setting, the BS aims to detect whether U_2 has sent a Gaussian signal with low or high variance by observing the total energy of the received signal. While the decision process takes place in the real and positive domain, deriving an exact theoretical model is difficult as the simultaneous presence of three overlapping signals, each influenced by complex fading, noise, and especially the correlation-shaped samples originating from U_3.

To begin, the BS computes the sample variance of the received signal using

$$s_y^2 = \frac{1}{N-1}\sum_{n=1}^{N} |y^n - \bar{y}|^2 , \tag{5.12}$$

where y^n is the nth complex-valued received sample and $\bar{y}$ is the sample mean.

The conditional variances of y^n, corresponding to bit-0 and bit-1 of U_2, are given by:

$$\begin{aligned} s_0^2 &= \sigma_1^2|h_1|^2 + \sigma_{2,l}^2|h_2|^2 + \eta P|h_3|^2 + \sigma_w^2, \\ s_1^2 &= \sigma_1^2|h_1|^2 + \sigma_{2,h}^2|h_2|^2 + \eta P|h_3|^2 + \sigma_w^2 \end{aligned} \tag{5.13}$$

The BS applies a decision rule that compares the observed sample variance s_y^2 with a reference threshold γ, which is chosen to balance the detection likelihoods under both bit hypotheses. This threshold can be computed optimally with the given conditional variances s_0^2 and s_1^2 as [Alshawaqfeh et al., 2024]

$$\gamma = \ln\left(\frac{s_1^2}{s_0^2}\right)\frac{s_1^2\, s_0^2}{s_1^2 - s_0^2}. \tag{5.14}$$

Then, the detection rule is:

$$\hat{b}_2 = \begin{cases} 0, & \text{if } s_y^2 < \gamma, \\ 1, & \text{if } s_y^2 > \gamma. \end{cases} \tag{5.15}$$

The conditional bit error probability (BEP) of U_2 is expressed as:

$$P_b = \frac{1}{2}P(s_y^2 > \gamma \mid b_2 = 0) + \frac{1}{2}P(s_y^2 < \gamma \mid b_2 = 1). \tag{5.16}$$

To analytically approximate this BEP for large N, we replace $\bar{y}$ in (5.12) with its expected value $\mathbb{E}[\bar{y}] = h_1 m_{1,i} + h_3 m_3$, yielding the approximation:

$$\begin{aligned} s_y^2 &\approx \frac{1}{N-1}\sum_{n=1}^{N} |y^n - h_1 m_{1,i} - h_3 m_3|^2 \\ &= \sum_{n=1}^{N} \Big[(y_R^n - h_{1,R} m_{1,i} - h_{3,R} m_3)^2 \\ &\quad + (y_I^n - h_{1,I} m_{1,i} - h_{3,I} m_3)^2 \Big]. \end{aligned} \tag{5.17}$$

By stacking the real and imaginary parts into a $2N \times 1$ real vector $\mathbf{y}$, this expression can be rewritten as a quadratic form:

$$s_y^2 = \mathbf{y}^T \Lambda \mathbf{y}, \tag{5.18}$$

where $\mathbf{y} \sim \mathcal{N}(0, \Sigma)$ and Λ is a diagonal matrix. Here, c denotes the covariance between the real and imaginary components of the received signal. The covariance matrix Σ includes real-valued variances and off-diagonal correlation terms between the real and imaginary components due to channel fading:

$$\Sigma = \begin{bmatrix} \sigma_R^2 & c & 0 & \cdots & 0 \\ c & \sigma_I^2 & 0 & \cdots & 0 \\ 0 & 0 & \ddots & & \vdots \\ \vdots & \vdots & & \sigma_R^2 & c \\ 0 & 0 & \cdots & c & \sigma_I^2 \end{bmatrix}_{2N \times 2N}, \tag{5.19}$$

Here, $\epsilon \triangleq \eta \cdot \frac{P}{\sigma_w^2}$ denotes the normalized power contribution of User-3's correlation-modulated signal relative to the noise power.

$$\begin{aligned} \sigma_R^2 &= h_{1,R}^2\sigma_1^2 + h_{2,R}^2\sigma_{2,k}^2 + \epsilon\sigma_w^2 h_{3,R}^2 + \frac{\sigma_w^2}{2}, \\ \sigma_I^2 &= h_{1,I}^2\sigma_1^2 + h_{2,I}^2\sigma_{2,k}^2 + \epsilon\sigma_w^2 h_{3,I}^2 + \frac{\sigma_w^2}{2}, \\ c &= h_{1,R}h_{1,I}\sigma_1^2 + h_{2,R}h_{2,I}\sigma_{2,k}^2 + \epsilon\sigma_w^2 h_{3,R}h_{3,I} \end{aligned} \tag{5.20}$$

Assuming N is large enough, we invoke the central limit theorem and approximate $s_y^2 \sim \mathcal{N}(\mu_s, \sigma_s^2)$, where

$$\begin{aligned} \mu_s &= \frac{N}{N-1}(\sigma_R^2 + \sigma_I^2), \\ \sigma_s^2 &= \frac{2N}{(N-1)^2}\left(\sigma_R^4 + \sigma_I^4 + 2c^2\right) \end{aligned} \tag{5.21}$$

Substituting into the BEP formula yields:

$$P_b = \frac{1}{2}Q\left(\frac{\gamma - \mu_{s|b_2=0}}{\sigma_{s|b_2=0}}\right) + \frac{1}{2}Q\left(\frac{\mu_{s|b_2=1} - \gamma}{\sigma_{s|b_2=1}}\right). \tag{5.22}$$

The threshold for equal error probabilities is

$$\gamma = \frac{\sigma_{s|b_2=0}\,\mu_{s|b_2=1} + \sigma_{s|b_2=1}\,\mu_{s|b_2=0}}{\sigma_{s|b_2=0} + \sigma_{s|b_2=1}}, \tag{5.23}$$

leading to a simplified BEP expression:

$$P_b = Q\left(\frac{\mu_{s|b_2=1} - \mu_{s|b_2=0}}{\sigma_{s|b_2=0} + \sigma_{s|b_2=1}}\right). \tag{5.24}$$

As with U_1, the conditional BEP of U_2 decays with increasing $\sqrt{N}$ due to the averaging in the variance estimate. However, due to the presence of multiple interfering signals and nonlinear dependence on channel coefficients, a closed-form expression for the unconditional BEP is not tractable. Therefore, numerical integration over the distributions of h_1, h_2, and h_3 is used. Despite the mathematical complexity, the detection process remains computationally simple, requiring only variance computation and comparison with a fixed threshold, which is expectedly a simpler detection model than traditional SIC-based demodulation.

5.1.4 Uplink – User 3 Detection

In the proposed ND-NOMA for three users uplink system, U_3 encodes its information bits by modulating the correlation between consecutive Gaussian samples. This method introduces a new dimension of modulation, referred to as correlation modulation, and allows U_3 to communicate independently of the mean and variance dimensions used by U_1 and U_2.

For each bit duration, U_3 transmits N real-valued Gaussian samples that are grouped into $N/2$ correlated pairs. These sample pairs are jointly drawn from a bivariate normal distribution with a specified correlation coefficient $\rho_k \in \{\rho_l, \rho_h\}$, corresponding to bit-0 and bit-1, respectively.

At the base station, the received signal is denoted as $\mathbf{y} = [y^1, y^2, \ldots, y^N]$, and is composed of contributions from all three users and noise. To recover U_3's bit, the base station divides $\mathbf{y}$ into two equal-length segments:

$$\mathbf{y}_1 = [y^1, \ldots, y^{N/2}], \quad \mathbf{y}_2 = [y^{N/2+1}, \ldots, y^N], \tag{5.25}$$

and calculates the empirical covariance between them:

$$\hat{\rho}_y = \frac{2}{N} \sum_{n=1}^{N/2} \mathrm{Re}\left\{(y^n - \bar{y}_1)(y^{n+N/2} - \bar{y}_2)^*\right\}, \tag{5.26}$$

where $\bar{y}_1$ and $\bar{y}_2$ are the respective sample means of $\mathbf{y}_1$ and $\mathbf{y}_2$. This estimator targets the underlying second-order correlation imposed by U_3's transmitted noise structure.

The base station then compares $\hat{\rho}_y$ to the expected correlation values under each hypothesis:

$$\begin{aligned} \hat{\rho}_l &= |h_3|^2 \rho_l \eta P, \\ \hat{\rho}_h &= |h_3|^2 \rho_h \eta P, \end{aligned} \tag{5.27}$$

where ηP represents the power allocated by U_3 and ρ_l, ρ_h are the correlation values used to modulate bit-0 and bit-1. The detection rule is a minimum distance test:

$$\hat{b}_3 = \begin{cases} 0, & \text{if } |\hat{\rho}_y - \hat{\rho}_l|^2 < |\hat{\rho}_y - \hat{\rho}_h|^2, \\ 1, & \text{if } |\hat{\rho}_y - \hat{\rho}_l|^2 > |\hat{\rho}_y - \hat{\rho}_h|^2. \end{cases} \tag{5.28}$$

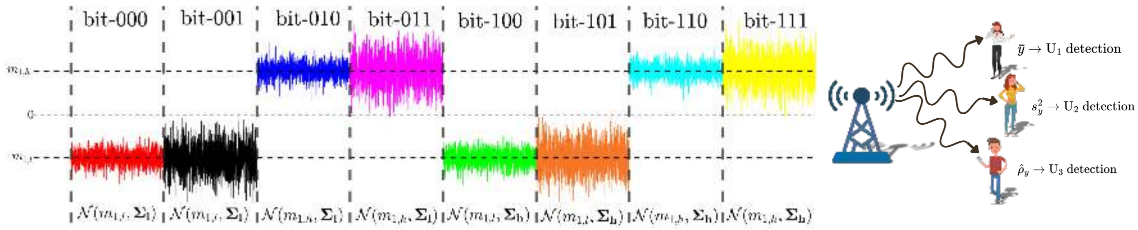

Figure 5.2: Downlink ND-NOMA scheme with three users using real Gaussian signals.

To characterize the BEP, we define a Gaussian random variable $D = \hat{\rho}_y - (\hat{\rho}_l + \hat{\rho}_h)/2$, and under the assumption of large N, D is approximately Gaussian due to averaging. Thus, the conditional BEP is written as:

$$P_b = Q\left(\frac{|\hat{\rho}_h - \hat{\rho}_l|}{2\sigma_C}\right), \tag{5.29}$$

where σ_C^2 is the variance of $\hat{\rho}_y$ and captures the uncertainty due to both interference and noise. Specifically, it includes contributions from all three users. Here, $\sigma_{1,C}^2$, $\sigma_{2,C}^2$, and $\sigma_{w,C}^2$ denote the contributions of U$_1$'s mean-modulated symbols, U$_2$'s variance modulation, and the additive channel noise, respectively, to the variance of the correlation estimate $\hat{\rho}_y$.:

$$\sigma_C^2 \approx \frac{1}{N/2}\left(\sigma_{1,C}^2 + \sigma_{2,C}^2 + \sigma_{w,C}^2\right). \tag{5.30}$$

These terms represent the impact of U$_1$'s mean-modulated samples, U$_2$'s variance modulation, and the additive channel noise. In practice, these variances are computed numerically in simulation using the channel realizations and transmitted bits.

Due to the complexity of closed-form expressions, the integral of the unconditional BEP is once again evaluated via Monte Carlo integration, as outlined in Appendix A. As observed in U$_1$ and U$_2$ detection, the conditional BEP of U$_3$ also decays with increasing N due to the law of large numbers, improving the accuracy of the empirical covariance estimation.

Table 5.1: Statistics of the transmitted and received signals for downlink ND-NOMA for three users

$\mathrm{U}_1/\mathrm{U}_2/\mathrm{U}_3$ bits	$s_{BS}^n \sim$	$y_i^n \sim$ for $i = 1, 2, 3$
000	$\mathcal{N}(m_l, \Sigma_{l,l})$	$\mathcal{CN}(h_i m_l, \lvert h_i\rvert^2\sigma_{2,l}^2 + \sigma_w^2)$
001	$\mathcal{N}(m_l, \Sigma_{h,l})$	$\mathcal{CN}(h_i m_l, \lvert h_i\rvert^2\sigma_{2,l}^2 + \sigma_w^2)$
010	$\mathcal{N}(m_l, \Sigma_{l,l})$	$\mathcal{CN}(h_i m_l, \lvert h_i\rvert^2\sigma_{2,h}^2 + \sigma_w^2)$
011	$\mathcal{N}(m_l, \Sigma_{h,l})$	$\mathcal{CN}(h_i m_l, \lvert h_i\rvert^2\sigma_{2,h}^2 + \sigma_w^2)$
100	$\mathcal{N}(m_h, \Sigma_{l,h})$	$\mathcal{CN}(h_i m_h, \lvert h_i\rvert^2\sigma_{2,l}^2 + \sigma_w^2)$
101	$\mathcal{N}(m_h, \Sigma_{h,h})$	$\mathcal{CN}(h_i m_h, \lvert h_i\rvert^2\sigma_{2,l}^2 + \sigma_w^2)$
110	$\mathcal{N}(m_h, \Sigma_{l,h})$	$\mathcal{CN}(h_i m_h, \lvert h_i\rvert^2\sigma_{2,h}^2 + \sigma_w^2)$
111	$\mathcal{N}(m_h, \Sigma_{h,h})$	$\mathcal{CN}(h_i m_h, \lvert h_i\rvert^2\sigma_{2,h}^2 + \sigma_w^2)$

5.2 Downlink Three User ND-NOMA: System Model and Performance Analysis

In this section, we present the downlink architecture of ND-NOMA for three users, where user data is simultaneously embedded into the mean, variance, and correlation of Gaussian noise samples.

5.2.1 System Model

As shown in Fig. 5.2, for the ND-NOMA for three users downlink scheme, the BS simultaneously serves three users by embedding their bits into different statistical domains of a common Gaussian noise signal. Specifically, U_1's bit is mapped to the mean of the noise samples, U_2's bit is encoded in the variance, and U_3's bit is represented through the correlation between consecutive sample pairs. Binary modulation is considered among each of the users. The complete statistical characterization of the transmitted and received signals for each possible bit combination in the downlink ND-NOMA for three users system is summarized in Table 5.1.

The BS transmits a sequence of N real-valued Gaussian noise samples per bit duration, with distribution defined as:

$$s_{BS}^{n} \sim \mathcal{N}(m_{1,i}, \boldsymbol{\Sigma_{k,j}}), \quad i, j, k \in \{l, h\}, \tag{5.31}$$

where $m_{1,i}$ is the bit-dependent mean associated with U_1 (bit $\mathrm{b}_{1,i}$), and σ_k^2 is the variance corresponding to U_2's bit $\mathrm{b}_{2,k}$. To embed U_3's information, we group the N real-valued samples into $N/2$ bivariate pairs. Each pair (s_{BS}^{2n-1}, s_{BS}^{2n}) uses a bit-dependent correlation coefficient $\rho_j \in \{\rho_l, \rho_h\}$. To jointly embed the bits of U_2 and U_3 in the noise domain, we define the combined covariance matrix as:

$$\boldsymbol{\Sigma}_{k,j} = \sigma_{2,k}^2 \begin{bmatrix} 1 & \rho_j \\ \rho_j & 1 \end{bmatrix}, \quad k, j \in \{l, h\} \tag{5.32}$$

This formulation captures the bit-dependent power allocation of U_2 through the variance term $\sigma_{2,k}^2$, and the bit-dependent correlation imposed by U_3 via ρ_j, resulting in a noise structure that encodes both users' information simultaneously.

The resulting noise sequence, jointly modulated in mean, variance, and correlation, is transmitted through fading channels. The received signals at the three users are:

$$y_1^n = h_1 s_{BS}^n + w_1^n, \tag{5.33.a}$$

$$y_2^n = h_2 s_{BS}^n + w_2^n, \tag{5.33.b}$$

$$y_3^n = h_3 s_{BS}^n + w_3^n, \tag{5.33.c}$$

for $n = 1, \ldots, N$. Here, h_1, h_2, and h_3 denote the complex downlink channel fading coefficients between the BS and each user, and $w_i^n \sim \mathcal{CN}(0, \sigma_w^2)$ is the AWGN at U_i for $i = 1, 2, 3$.

We assume the BS transmits with a total power budget of P, such that:

$$\mathbb{E}[(s_{BS}^n)^2] = P. \tag{5.34}$$

To divide this power among the three users, we define a power partitioning parameter ψ for U_1 and $(1 - \psi)$ for the remaining variance and correlation modulation. More specifically, the mean of the signal is allocated a portion ψ of the total power (DC component), and the variance, which supports both U_2 and U_3, receives $(1 - \psi)P$

(AC component). The bit-dependent means satisfy $m_{1,h} = -m_{1,l}$ and $m_{1,l}^2 = \psi P$, while the variances are chosen such that:

$$\frac{\sigma_{2,l}^2 + \sigma_{2,h}^2}{2} = (1-\psi)P, \quad \sigma_{2,h}^2 = \alpha \sigma_{2,l}^2. \tag{5.35}$$

To facilitate correlation modulation, each pair of noise samples has a correlation coefficient ρ_j determined by U_3's bit. These correlation values are selected such that the second moment of each sample remains within the overall power constraint, preserving the total energy allocated to the ac component.

Unlike in uplink ND-NOMA, the downlink signals do not overlap in terms of physical transmission — a single superimposed signal is broadcast by the BS. However, since each user extracts their bit from a different statistical property of the signal, there is no need for SIC, and detection can be performed independently at each receiver using straightforward statistical operations. As a result, the downlink ND-NOMA system benefits from reduced complexity and avoids typical error propagation problems encountered in PD-NOMA systems.

In the subsequent sections, we detail the detection mechanisms used by each user to extract their respective information from the received signal and provide analytical expressions for their corresponding BEP.

5.2.2 Downlink – User 1 Detection

In the downlink transmission of the ND-NOMA for three users scheme, U_1 recovers its bit by exploiting the mean modulation embedded by the BS in the transmitted noise samples. This detection mechanism mirrors that of the uplink, but the composite interference now also includes contributions from both U_2's variance modulation and U_3's correlation-based structure.

$\bar{y}_R$ and $\bar{y}_I$ denote the real and imaginary components of $\bar{y}$, respectively. Their individual variances and covariance are

$$\begin{aligned}
\mathrm{VAR}[\bar{y}_R] &= \frac{1}{N}\left(h_{1,R}^2\,\sigma_1^2 + h_{2,R}^2\,\sigma_{2,k}^2 + \frac{\beta P^2}{\sigma_w^2}\,h_{3,R}^2 + \frac{\sigma_w^2}{2}\right),\\
\mathrm{VAR}[\bar{y}_I] &= \frac{1}{N}\left(h_{1,I}^2\,\sigma_1^2 + h_{2,I}^2\,\sigma_{2,k}^2 + \frac{\beta P^2}{\sigma_w^2}\,h_{3,I}^2 + \frac{\sigma_w^2}{2}\right),\\
\mathrm{COV}[\bar{y}_R,\bar{y}_I] &= \frac{1}{N}\left(h_{1,R}h_{1,I}\,\sigma_1^2 + h_{2,R}h_{2,I}\,\sigma_{2,k}^2 + \frac{\beta P^2}{\sigma_w^2}\,h_{3,R}h_{3,I}\right),
\end{aligned} \tag{5.36}$$

where $m_{1,i} \in \{m_{1,l}, m_{1,h}\}$ is the bit-dependent mean used by the BS to represent U_1's bit, and $\sigma_{2,k}^2$ is the variance selected based on U_2's bit. The term $\frac{\beta P^2}{\sigma_w^2}$ accounts for the power allocated to U_3's correlation-modulated signal, which appears as structured interference at all users, scaled by the downlink channel coefficient h_1.

Given this distribution, the optimal minimum-distance detector for U_1 is expressed as:

$$\hat{b}_1 = \begin{cases} 0, & \text{if } |\bar{y}_1 - h_1 m_{1,l}|^2 < |\bar{y}_1 - h_1 m_{1,h}|^2, \\ 1, & \text{if } |\bar{y}_1 - h_1 m_{1,l}|^2 > |\bar{y}_1 - h_1 m_{1,h}|^2. \end{cases} \tag{5.37}$$

This rule leads to the following expression for the conditional BEP:

$$\begin{aligned}
P_b &= P\left(|\bar{y}_1 - h_1 m_{1,h}|^2 < |\bar{y}_1 - h_1 m_{1,l}|^2 \mid b_1 = 0\right)\\
&= P\left(\mathrm{Re}\{\bar{y}_1 h_1^* m_{1,l}\} < 0 \mid b_1 = 0\right)\\
&= Q\left(\frac{m_D}{\sigma_D}\right),
\end{aligned} \tag{5.38}$$

where $D = \mathrm{Re}\{\bar{y}_1 h_1^* m_{1,l}\}$ is a real Gaussian variable with

$$\begin{aligned}
m_D &= |h_1|^2 m_{1,l}^2,\\
\sigma_D^2 &= m_{1,l}^2\left(h_{1,R}^2 \mathrm{VAR}[\bar{y}_{1,R}] + h_{1,I}^2 \mathrm{VAR}[\bar{y}_{1,I}]\right.\\
&\qquad \left. + 2h_{1,R}h_{1,I}\mathrm{COV}(\bar{y}_{1,R},\bar{y}_{1,I})\right)
\end{aligned} \tag{5.39}$$

The variances and covariance of the real and imaginary parts of $\bar{y}_1$ are given by:

$$\begin{aligned}
\mathrm{VAR}[\bar{y}_{1,R}] &= \frac{1}{N}\left(h_{1,R}^2\sigma_{2,k}^2 + \frac{\beta P^2}{\sigma_w^2}h_{1,R}^2 + \frac{\sigma_w^2}{2}\right),\\
\mathrm{VAR}[\bar{y}_{1,I}] &= \frac{1}{N}\left(h_{1,I}^2\sigma_{2,k}^2 + \frac{\beta P^2}{\sigma_w^2}h_{1,I}^2 + \frac{\sigma_w^2}{2}\right),\\
\mathrm{COV}(\bar{y}_{1,R},\bar{y}_{1,I}) &= \frac{1}{N}\left(h_{1,R}h_{1,I}\sigma_{2,k}^2 + \frac{\beta P^2}{\sigma_w^2}h_{1,R}h_{1,I}\right)
\end{aligned} \tag{5.40}$$

Substituting these into the expression for σ_D^2 yields the full conditional BEP for U_1.

Finally, as in the uplink case, the unconditional BEP is obtained via numerical averaging over the fading distribution of h_1, as well as over the equiprobable values of $\sigma_{2,k}^2$. The resulting performance illustrates that, despite the added interference from U_3, U_1's detection remains efficient due to its orthogonal mapping into the mean of the signal.

5.2.3 Downlink – User 2 Detection

In the downlink phase of the ND-NOMA for three users system, U_2 extracts its bit from the variance of the received signal, in a fashion similar to the uplink detection scheme. However, the downlink environment introduces a different interference pattern since the transmitted signal now embeds the bits of all users in a single waveform. While U_2 still detects variance changes, its observation is affected by both U_1's mean modulation and U_3's correlation modulation.

To begin, the receiver at U_2 computes the sample variance of the received signal over N samples:

$$s_{y_2}^2 = \frac{1}{N-1} \sum_{n=1}^{N} |y_2^n - \bar{y}_2|^2 , \tag{5.41}$$

where $\bar{y}_2 = \frac{1}{N}\sum_{n=1}^{N} y_2^n$ is the sample mean. Based on the signal structure, the received signal is impacted by the mean and variance chosen by the BS according to U_1 and U_2's bits, and further distorted by U_3's correlation-induced sample structure. This results in conditional variance expressions:

$$\begin{aligned} s_0^2 &= |h_2|^2\sigma_{2,l}^2 + |h_2|^2(1-\psi)P + \sigma_w^2, \\ s_1^2 &= |h_2|^2\sigma_{2,h}^2 + |h_2|^2(1-\psi)P + \sigma_w^2, \end{aligned} \tag{5.42}$$

where $\sigma_{2,l}^2$ and $\sigma_{2,h}^2$ represent the bit-dependent variances for U_2, and $(1-\psi)P$ denotes the average power contribution of U_3's signal, which adds structured variance interference that scales with $|h_2|^2$.

To decide between the two variance hypotheses, U_2 applies a threshold test:

$$\hat{b}_2 = \begin{cases} 0, & \text{if } s_{y_2}^2 < \gamma, \\ 1, & \text{if } s_{y_2}^2 > \gamma, \end{cases} \tag{5.43}$$

with threshold γ, which can be calculated optimally as [Alshawaqfeh et al., 2024]

$$\gamma = \ln\left(\frac{s_1^2}{s_0^2}\right)\frac{s_1^2\, s_0^2}{s_1^2 - s_0^2}. \tag{5.44}$$

The conditional BEP becomes:

$$P_b = \frac{1}{2}P(s_{y_2}^2 > \gamma \mid b_2 = 0) + \frac{1}{2}P(s_{y_2}^2 < \gamma \mid b_2 = 1). \tag{5.45}$$

To analyze this statistically, we approximate $s_{y_2}^2 \approx \frac{1}{N-1}\sum_{n=1}^{N}|y_2^n - h_2 m_{1,i}|^2$, replacing $\bar{y}_2$ by its conditional expectation $\mathbb{E}[\bar{y}_2] = h_2 m_{1,i}$ as done in the uplink model. This lets us express $s_{y_2}^2$ as a quadratic form of a $2N \times 1$ real Gaussian vector:

$$s_{y_2}^2 = \mathbf{y}^T \Lambda \mathbf{y}, \tag{5.46}$$

where $\mathbf{y} \sim \mathcal{N}(0, \Sigma)$, and Λ is a diagonal matrix. The covariance matrix Σ remains banded and is updated for the current scenario:

$$\Sigma = \begin{bmatrix} \sigma_R^2 & c & 0 & \cdots & 0 \\ c & \sigma_I^2 & 0 & \cdots & 0 \\ 0 & 0 & \ddots & & \vdots \\ \vdots & \vdots & & \sigma_R^2 & c \\ 0 & 0 & \cdots & c & \sigma_I^2 \end{bmatrix}, \tag{5.47}$$

with:

$$\begin{aligned} \sigma_R^2 &= h_{2,R}^2\sigma_{2,k}^2 \ + \ (1-\psi)P\, h_{2,R}^2 \ + \ \frac{\sigma_w^2}{2}, \\ \sigma_I^2 &= h_{2,I}^2\sigma_{2,k}^2 \ + \ (1-\psi)P\, h_{2,I}^2 \ + \ \frac{\sigma_w^2}{2}, \\ c &= h_{2,R}h_{2,I}\sigma_{2,k}^2 \ + \ (1-\psi)P\, h_{2,R}h_{2,I}. \end{aligned} \tag{5.48}$$

for $k \in \{l, h\}$, depending on the bit transmitted.

Assuming sufficiently large N, we invoke the central limit theorem and approximate $s_{y_2}^2 \sim \mathcal{N}(\mu_s, \sigma_s^2)$ with:

$$\begin{aligned} \mu_s &= \frac{N}{N-1}(\sigma_R^2 + \sigma_I^2), \\ \sigma_s^2 &= \frac{2N}{(N-1)^2}(\sigma_R^4 + \sigma_I^4 + 2c^2). \end{aligned} \tag{5.49}$$

Substituting into the BEP equation, we obtain:

$$P_b = \frac{1}{2}Q\left(\frac{\gamma - \mu_{s|b_2=0}}{\sigma_{s|b_2=0}}\right) + \frac{1}{2}Q\left(\frac{\mu_{s|b_2=1} - \gamma}{\sigma_{s|b_2=1}}\right). \tag{5.50}$$

The optimal threshold γ for equal error probabilities is:

$$\gamma = \frac{\sigma_{s|b_2=0}\mu_{s|b_2=1} + \sigma_{s|b_2=1}\mu_{s|b_2=0}}{\sigma_{s|b_2=0} + \sigma_{s|b_2=1}}, \tag{5.51}$$

and the simplified expression for BEP becomes:

$$P_b = Q\left(\frac{\mu_{s|b_2=1} - \mu_{s|b_2=0}}{\sigma_{s|b_2=0} + \sigma_{s|b_2=1}}\right). \tag{5.52}$$

As with the uplink case, the conditional BEP decays with increasing N, and the unconditional BEP is computed via numerical integration over the fading coefficients h_2 and U_3's interference profile. Despite the added complexity from U_3, the detection remains computationally light and does not require interference cancellation.

5.2.4 Downlink – User 3 Detection

In the ND-NOMA for three users downlink system, U_3 decodes its bit based on correlation modulation—mirroring the structure used in the uplink case. Specifically, the BS encodes U_3's information into the correlation between consecutive noise samples. Each bit of U_3 is transmitted by shaping the joint distribution of N real-valued noise samples into $N/2$ bivariate Gaussian pairs with low or high correlation, corresponding to bit-0 and bit-1, respectively.

The transmitted signal $s_{BS}^n \sim \mathcal{N}(m_{1,i}, \mathbf{\Sigma}_{k,j})$ is further structured such that each sample pair $(s_{BS}^{2n-1}, s_{BS}^{2n})$ follows a bivariate normal distribution with correlation coefficient $\rho_j \in \{\rho_l, \rho_h\}$ depending on the bit of U_3. The received signal at U_3 is modeled as it was in (5.33.c).

To extract the embedded bit through correlation, U_3 splits its received vector into two halves:

$$\mathbf{y}_1 = [y_3^1, \ldots, y_3^{N/2}], \quad \mathbf{y}_2 = [y_3^{N/2+1}, \ldots, y_3^N],$$

and computes the real part of the sample correlation estimate:

$$\hat{\rho}_y = \frac{2}{N}\sum_{n=1}^{N/2} \mathrm{Re}\left\{(y_3^n - \bar{y}_1)(y_3^{n+N/2} - \bar{y}_2)^*\right\}, \tag{5.53}$$

where $\bar{y}_1$ and $\bar{y}_2$ denote the sample means of the respective halves. This statistic estimates the correlation introduced at the transmitter and distorted by fading and additive noise.

The BS's correlation structure results in two reference correlation levels at the receiver:

$$\begin{aligned} \hat{\rho}_l &= |h_3|^2 \rho_l \,(1-\psi)P, \\ \hat{\rho}_h &= |h_3|^2 \rho_h \,(1-\psi)P. \end{aligned} \tag{5.54}$$

Based on these references, the detection rule is given by

$$\hat{b}_3 = \begin{cases} 0, & \text{if } |\hat{\rho}_y - \hat{\rho}_l|^2 < |\hat{\rho}_y - \hat{\rho}_h|^2, \\ 1, & \text{if } |\hat{\rho}_y - \hat{\rho}_l|^2 > |\hat{\rho}_y - \hat{\rho}_h|^2. \end{cases} \tag{5.55}$$

Assuming $\hat{\rho}_y$ is approximately Gaussian due to averaging over a large number of samples, the conditional bit error probability becomes:

$$P_b = Q\left(\frac{|\hat{\rho}_h - \hat{\rho}_l|}{2\sigma_C}\right), \tag{5.56}$$

where σ_C^2 denotes the variance of $\hat{\rho}_y$. This variance captures the impact of U_1's mean, U_2's variance modulation, and noise, all passed through the same fading channel h_3. An analytical approximation for the covariance variance is given by:

$$\sigma_C^2 \approx \frac{1}{N/2}\left(\sigma_{1,C}^2 + \sigma_{2,C}^2 + \sigma_{w,C}^2\right), \tag{5.57}$$

where each term quantifies the covariance uncertainty due to mean interference (from U_1), variance interference (from U_2), and thermal noise.

Since a closed-form solution for the unconditional BEP is analytically intractable, as detailed in Appendix A, integration over the Rician fading coefficients to estimate the unconditional BEP.

5.3 Numerical Results

In this section, we examine the BER performance of the proposed ND-NOMA for three users system for both uplink and downlink scenarios. We assume that each user's wireless channel is subject to Rician fading. To obtain average BEP values

Table 5.2: Simulation Parameters for 3-User ND-NOMA System

Parameter	**Value**
δ_{dB}	[-30, 10] , [-40, 10]
α	10
P_{dBm}	40
β	1/100 (UL), 1/1024 (DL)
ρ	-1, +1
ψ	0.5

across fading conditions, we adopt the Monte Carlo integration technique whose details are given in Appendix A. This approach enables accurate evaluation of the unconditional BEP for all users under realistic channel conditions. The simulation outcomes are compared with theoretical predictions to validate the effectiveness of the system. Simulation parameters used throughout the analysis are presented in Table 5.2.

5.3.1 Uplink Scenario

Figs. 5.3 and 5.4 illustrate the uplink BER performance of U_1, U_2 and U_3. The BS jointly receives the superimposed signals from all users under a Rician fading channel, with varying noise configurations. Figs. 5.3(a) and 5.3(b) shows the BER performance of the three users for $N = 150$ and $N = 200$ samples, respectively, under a fixed Rician K-factor of $K = 10$ dB.

It is observed that U_1 achieves the lowest BER among all users due to its use of mean modulation, which is more robust to noise and channel variations. On the other hand, U_2 and U_3, employing variance- and correlation-based modulation respectively, exhibit relatively higher BERs. This is mainly because their detection relies on more sensitive statistical features, which are more easily affected by in-

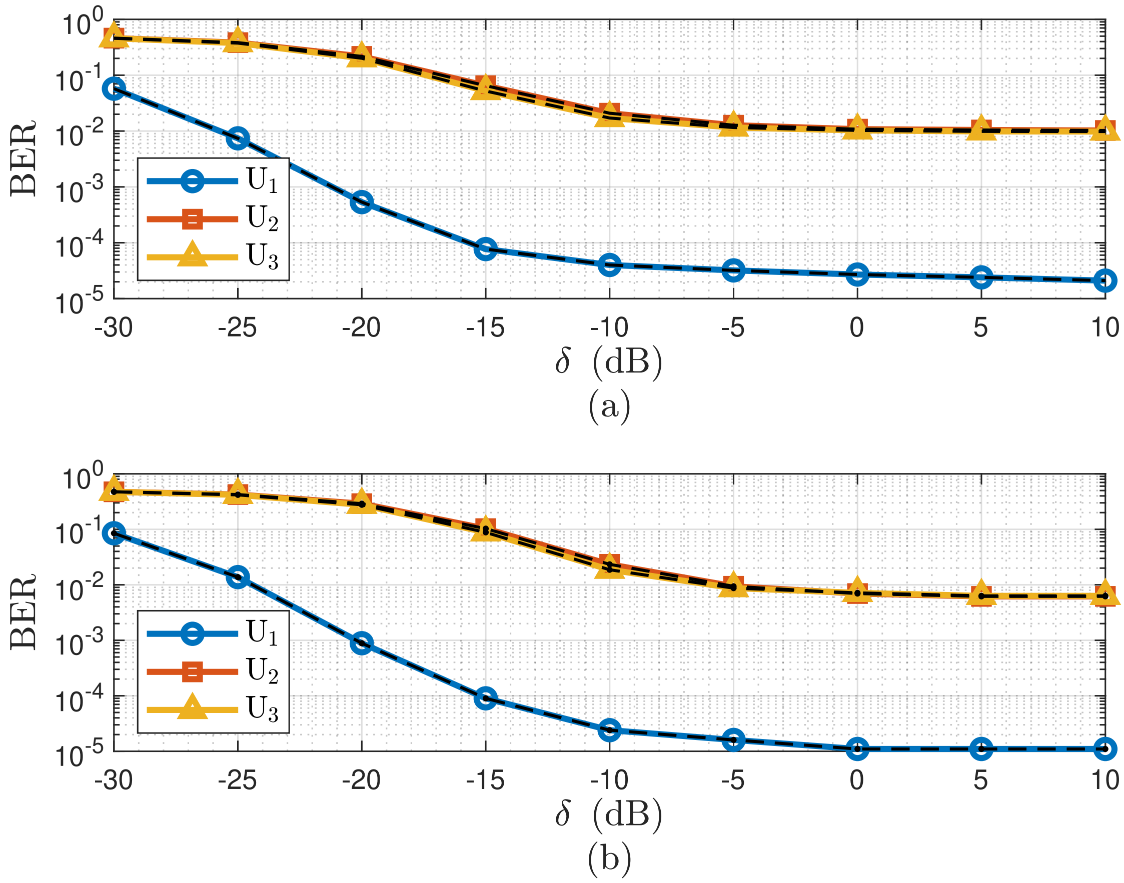

Figure 5.3: Simulated BER and theoretical BEP (shown as dashed black lines) for the uplink ND-NOMA for three users system versus δ, under Rician fading with $K = 10$ dB. Results are shown for (a) $N = 150$ and (b) $N = 200$ samples.

terference and noise. Ultimately it must be stated that expectedly, increasing the number of noise samples from $N = 150$ to $N = 200$ improves BER performance for all users, as larger N provides more reliable statistical estimates at the receiver.

As expected, increasing δ leads to improved BER performance for all users. A higher δ implies stronger signal components relative to noise, making it easier for the receiver to distinguish.

Fig. 5.4 extends the analysis by comparing uplink BER performance for two different Rician K-factors, namely $K = 5$ dB and $K = 10$ dB where N is fixed to 200. As expected, stronger line-of-sight conditions (higher K) lead to improved performance for all users, validating the analytical model's accuracy across channel conditions. The theoretical BEP expressions align well with simulation results,

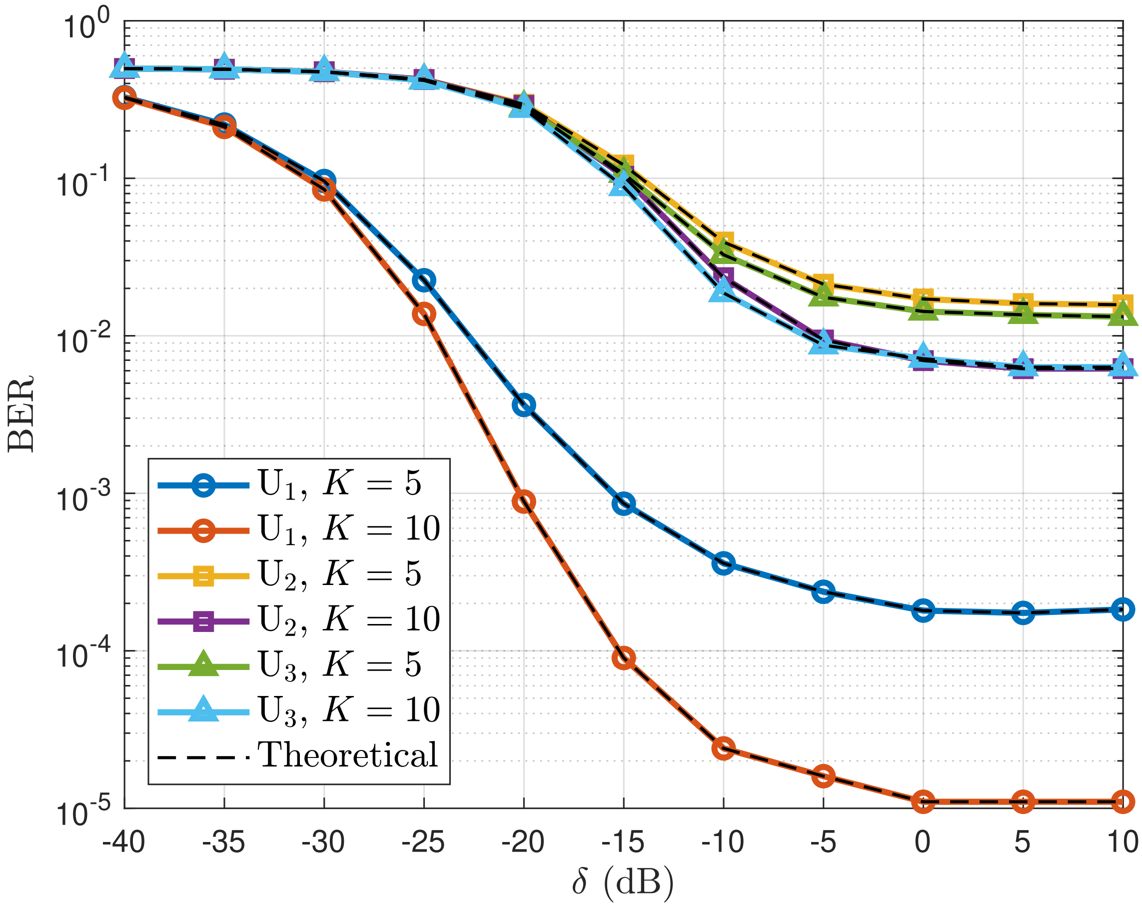

Figure 5.4: Theoretical BEP and simulated BER for uplink ND-NOMA versus δ with Rician K-factors of 5 and 10.

confirming the validity of our approximations.

5.3.2 Downlink Scenario

Figs. 5.5 and 5.6 illustrate the BER performance of U_1, U_2, and U_3 in the downlink ND-NOMA system, where each user recovers their bit independently using simple detection rules. Fig. 5.5(a) and Fig. 5.5(b) display BER results for $N = 150$ and $N = 200$ samples, respectively, while Fig. 5.6 compares performance across different Rician K-factors, with $K \in \{5, 10\}$ dB at a fixed $N = 200$.

As shown in Figs. 5.5(a) and 5.5(b), U_1 achieves the best performance among all users just like the uplink scenario, benefiting from the robustness of mean-based detection under noise and fading. In contrast, U_2 and U_3 show relatively higher BERs

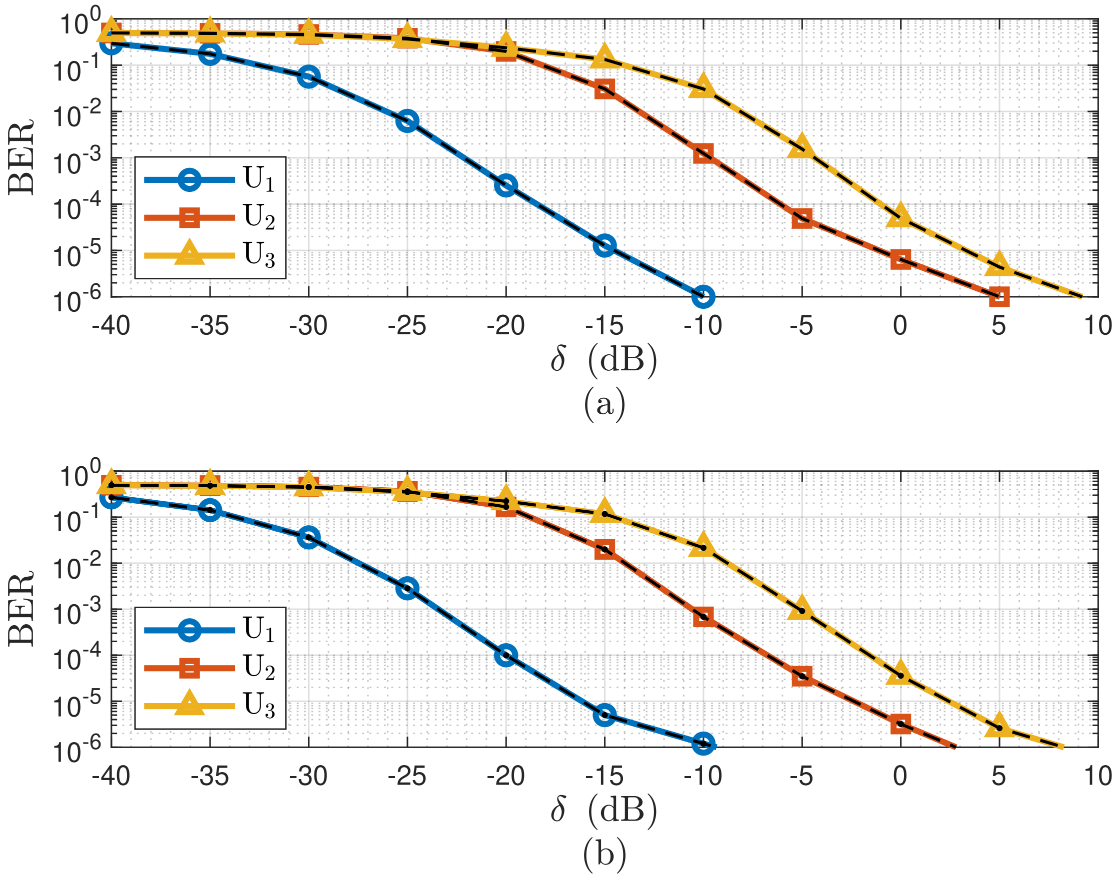

Figure 5.5: Simulated BER and theoretical BEP (shown as dashed black lines) for the downlink ND-NOMA for three users system versus δ, under Rician fading with $K = 10$ dB. Results are shown for (a) $N = 150$ and (b) $N = 200$ samples.

due to their reliance on variance and correlation features, which are more susceptible to interference and statistical estimation error. Notably, U_3 slightly outperforms U_2 in the downlink case. This is attributed to the fact that correlation-based detection, while sensitive, benefits from the symmetrical structure of the broadcast signal, and offers simpler bit-level decisions based on a single statistic. Increasing the number of noise samples and δ improves BER performance for all users once again, as larger sample sizes yield more accurate statistical estimates.

Fig. 5.6 further supports this by demonstrating that a higher Rician K-factor improves performance for all users. With $K = 10$ dB providing stronger line-of-sight conditions than $K = 5$ dB, resulting in lower BER. The exact match between theoretical and simulated curves confirms the accuracy of the analytical model in

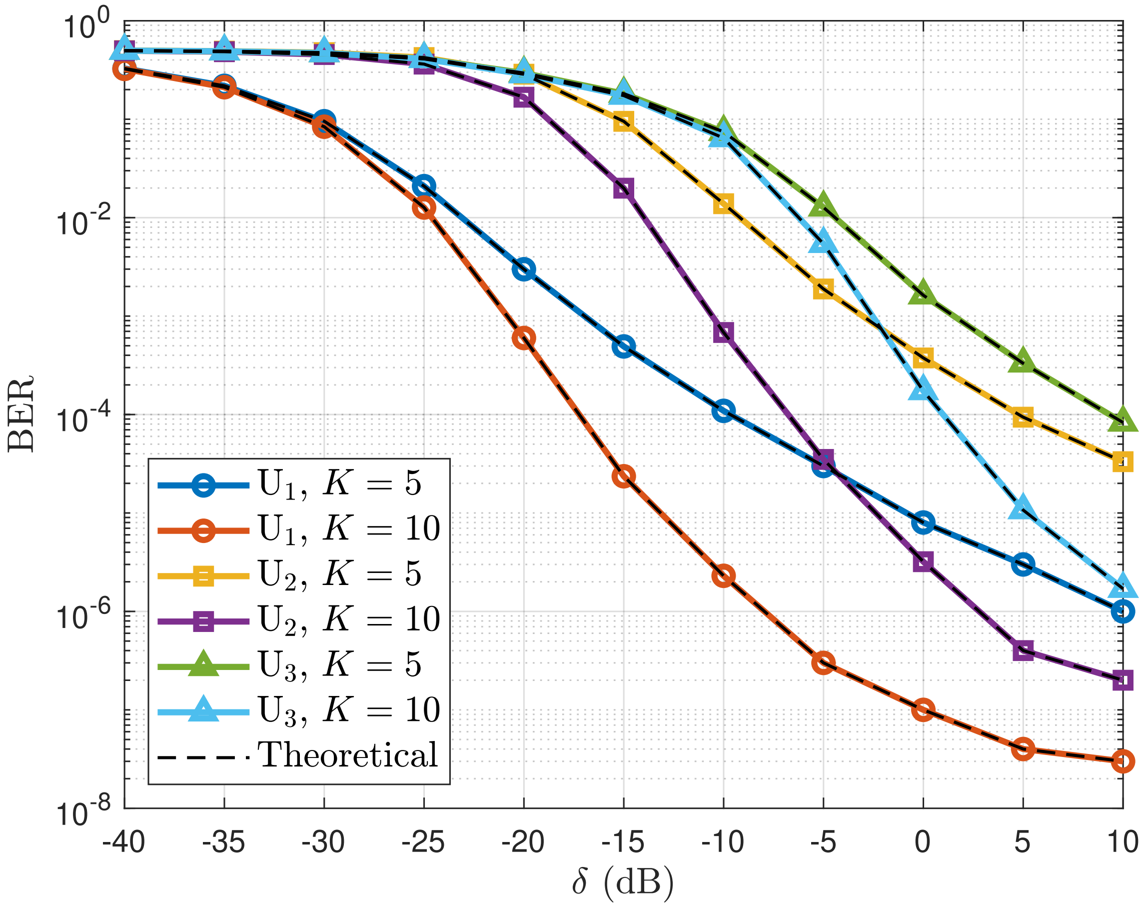

Figure 5.6: Theoretical BEP and simulated BER for downlink ND-NOMA versus δ with Rician K-factors of 5 and 10.

characterizing the downlink system. Furthermore, the satisfactory BER performance observed across users in the downlink scenario stems from the absence of mutual interference, as each user's information is embedded in orthogonal statistical domains, enabling reliable detection without the need for complex receiver processing.

Chapter 6

CONCLUSION

In this thesis, three novel noise-domain communication frameworks were introduced to address the limitations of the conventional modulation methods and multiple access techniques in low-power and low-adata-rate IoT applications. These schemes utilize the statistical properties of Gaussian noise, which are mean, variance, and correlation as carriers of information, eliminating the need for SIC, frequency synchronization, and power allocation.

Initially, a Joint Energy and Information Harvesting scheme using Noise Modulation was proposed to embed information into the mean of Gaussian noise samples while enabling energy harvesting at the receiver through a time-switching approach. Analytical expressions for the BEP were derived under Rician fading and nonlinear rectenna models. Simulation results have shown that JEIH-Noise Mod specifically enhances the energy harvesting capability without sacrificing the BER performance, making it well-suited for the energy-constrained semi-passive IoT devices.

Secondly, a ND-NOMA scheme was proposed, where data of the two user are multiplexed using the mean and variance of the noise samples. Unlike PD-NOMA, ND-NOMA eliminates the need for SIC at the receiver side, which simplifies the receiver architecture. The system was analyzed under the Rayleigh and Rician fading scenarios. Our simulation results confirmed the low BER and efficiency of ND-NOMA, especially for the Device Type B IoT use cases, which prioritize minimal hardware complexity and energy usage.

Ultimately, a new ND-NOMA framework was proposed, which supported a three-user scenario by introducing correlation modulation as a third orthogonal dimension alongside mean and variance. The resulting system enables simultaneous transmission of the data of the three users at the same time. Both theoretical and simulation-based analyses confirmed the scalability and the reliability of this scheme in various channel environments.

Collectively, these contributions show the potential of noise-domain communication systems as viable solutions for next-generation IoT networks. The simplicity of receiver design, compatibility with energy harvesting, and elimination of synchronization requiremets position these methods as strong candidates for future 6G and ultra-low-power wireless applications.

6.1 Publications Derived from This Thesis

As a result of the work carried out in this thesis, the following research papers have been published or are under review.

1. E. Yapici, Y. I. Tek, M. E. Pihtili, M. C. Ilter, and E. Basar, "Noise modulation over wireless energy transfer: JEIH-Noise Mod," IEEE Wirel. Commun. Lett., Jun. 2025, early access

2. "Noise-Domain Non-Orthogonal Multiple Access" under review at *IEEE Open Journal of the Communications Society.*

3. "Noise-Domain Non-Orthogonal Multiple Access for Three Users" under review at *IEEE Transactions on Wireless Communications.*

BIBLIOGRAPHY

[Alshawaqfeh et al., 2024] Alshawaqfeh, M. K., Badarneh, O. S., Al-Badarneh, Y. H., Dabiri, M. T., and Hasna, M. O. (2024). Thermal noise modulation: Optimal detection and performance analysis. *IEEE Commun. Lett.*, 28(12):2930–2934.

[Anand, 2019] Anand, T. (2019). A stochastic wireline communication system. In *Proc. 2019 IEEE Int. Midwest Symp. Circuits Syst.*, Dallas, TX, USA.

[Ashraf et al., 2021] Ashraf, N., Sheikh, S. A., Khan, S. A., Shayea, I., and Jalal, M. (2021). Simultaneous wireless information and power transfer with cooperative relaying for next-generation wireless networks: A review. *IEEE Access*, 9:71482–71504.

[Basar, 2023] Basar, E. (2023). Communication by means of thermal noise: Towards networks with extremely low power consumption. *IEEE Trans. Wirel. Commun*, 71(2):688–699.

[Basar, 2024] Basar, E. (2024). Noise modulation. *IEEE Wirel. Commun. Lett.*, 13(3):844–848.

[Basnayaka and Haas, 2017] Basnayaka, D. A. and Haas, H. (2017). A new degree of freedom for energy efficiency of digital communication systems. *IEEE Trans. Commun.*, 65(7):3023–3036.

[Butt et al., 2024] Butt, M. M., Mangalvedhe, N. R., Pratas, N. K., Harrebek, J., Kimionis, J., Tayyab, M., Barbu, O.-E., Ratasuk, R., and Vejlgaard, B. (2024). Ambient IoT: A missing link in 3GPP IoT devices landscape. *IEEE Internet Things Mag.*, 7(2):85–92.

[Clerckx and Bayguzina, 2016] Clerckx, B. and Bayguzina, E. (2016). Waveform design for wireless power transfer. *IEEE Trans. Signal Process.*, 64(23):6313–6328.

[Ding et al., 2014] Ding, Z., Yang, Z., Fan, P., and Poor, H. V. (2014). On the performance of non-orthogonal multiple access in 5G systems with randomly deployed users. *IEEE Signal Process. Lett.*, 21(12):1501–1505.

[F. Jameel and Lee, 2019] F. Jameel, T. Ristaniemi, I. K. and Lee, B. M. (2019). Simultaneous harvest-and-transmit ambient backscatter communications under rayleigh fading. *J. Wireless Commun. Netw.*, 2019(166):1–9.

[Kim et al., 2020] Kim, J., Clerckx, B., and Mitcheson, P. D. (2020). Signal and system design for wireless power transfer: Prototype, experiment and validation. *IEEE Trans. Wireless Commun.*, 19(11):7453–7469.

[Kish, 2005] Kish, L. B. (2005). Stealth communication: Zero-power classical communication, zero-quantum quantum communication and environmental-noise communication. *Appl. Phys. Lett.*, 87(23):234109.

[Kish, 2006] Kish, L. B. (2006). Totally secure classical communication utilizing Johnson (-like) noise and Kirchoff's law. *Phys. Lett. A*, 352:178–182.

[Koivunen et al., 2024] Koivunen, V., Keskin, M. F., Wymeersch, H., Valkama, M., and González-Prelcic, N. (2024). Multicarrier ISAC: Advances in waveform design, signal processing and learning under non-idealities. *arXiv preprint arXiv:2406.18476*.

[Kozlendrakov and Boysi, 2018] Kozlendrakov, M. and Boysi, A. (2018). Performance of spread spectrum system with noise shift keying using entropy demodulation. In *Proc. 2018 14th Int. Conf. Advanced Trends Radioteleconf. Telecommun. Computer Eng.*, Lviv-Slavske, Ukraine.

[Kramer and Bessai, 2017] Kramer, M. and Bessai, H. (2017). Sigma shift keying (SSK): A paradigm shift in digital modulation techniques. In *Proc. 2017 2nd Int. Conf. Computer Commun. Syst.*, pages 60–64, Krakow, Poland.

[Mathai and Provost, 1992] Mathai, A. and Provost, S. B. (1992). *Quadratic Forms in Random Variables: Theory and Applications.* Marcel Dekker, New York, NY, USA.

[Paolella, 2018] Paolella, M. (2018). *Linear Models and Time-Series Analysis: Regression, ANOVA, ARMA and GARCH.* Wiley, New York, NY, USA.

[Pihtili et al., 2024] Pihtili, M. E., Ilter, M. C., Basar, E., Wichman, R., and Hämäläinen, J. (2024). Index modulation-based information harvesting for far-field RF power transfer. *IEEE Trans. Wirel. Commun.*, 23(10):14895–14909.

[Press, 2007] Press, W. (2007). *Numerical Recipes 3rd Edition: The Art of Scientific Computing.* Cambridge University Press.

[Salbert and Hanssen, 1999] Salbert, A.-B. and Hanssen, A. (1999). Secure digital communications by means of stochastic process shift keying. In *Proc. Conf. Rec. 33rd Asilomar Conf. Signals, Syst., Comput.*, volume 2, pages 1523–1527, Pacific Grove, CA, USA.

[Song et al., 2014] Song, C., Ling, C., Park, J., and Clerckx, B. (2014). MIMO broadcasting for simultaneous wireless information and power transfer: Weighted MMSE approaches. In *2014 IEEE Globecom Workshops, GC Wkshps 2014*, volume 12, pages 1151–1156. IEEE.

[Xu et al., 2017] Xu, Z., Gong, Y., Wang, K., et al. (2017). Covert digital communication systems based on joint normal distribution. *IET Commun.*, 11(8):1282–1290.

[Yapici et al., 2024] Yapici, E., Tek, Y. I., and Basar, E. (2024). Noise-domain non-orthogonal multiple access.

[Yapici et al., 2025] Yapici, E., Tek, Y. I., Pihtili, M. E., Ilter, M. C., and Basar, E. (2025). Noise modulation over wireless energy transfer: JEIH-NoiseMod. *IEEE Wirel. Commun. Lett.* early access.

[Yuan et al., 2020] Yuan, R., Ma, J., Su, P., Dong, Y., and Cheng, J. (2020). Monte-Carlo integration models for multiple scattering based optical wireless communication. *IEEE Trans. Commun.*, 68(1):334–348.

[Zhou et al., 2013] Zhou, X., Zhang, R., and Ho, C. K. (2013). Wireless information and power transfer: Architecture wireless information and power transfer: Architecture design and rate-energy tradeoff design and rate-energy tradeoff. *IEEE Trans. Commun.*, 61(11):4754–4767.

Appendix A

A.1 Monte Carlo Integration Method

Monte Carlo integration is a powerful technique for numerically estimating integrals, particularly in high-dimensional spaces or when the integrand has a complex form. In this appendix, we have addressed the problem of unconditional BEP integrals mentioned in previous sections. As an initial step, we can rewrite (4.9) as

$$\bar{P}_b = \int_V g(h_{1,R}, h_{1,I}, h_{2,R}, h_{2,I}) d\hat{h}, \tag{A.1}$$

where

$$g(h_{1,R}, h_{1,I}, h_{2,R}, h_{2,I}) = P_b f(h_{1,R}) f(h_{1,I}) f(h_{2,R}) f(h_{2,I})$$

and $d\hat{h} = dh_{1,R} dh_{1,I} dh_{2,R} dh_{2,I}$. Here, V is the whole integration volume. Then, we will utilize importance sampling to compute the integral efficiently. We choose an appropriate joint PDF $z(h_{1,R}, h_{1,I}, h_{2,R}, h_{2,I})$ that matches the form of the integrand as

$$z(h_{1,R}, h_{1,I}, h_{2,R}, h_{2,I}) = z(h_{1,R}) z(h_{1,I}) z(h_{2,R}) z(h_{2,I}), \tag{A.2}$$

where $z(\cdot)$ denotes the sampling function in the integral volume $V(z > 0, \int_V f_n \, \mathrm{d}V = 1)$. Specifically, $z(\cdot)$ represents a PDF characterized by the same mean and variance as the PDFs of channel gains $f(\cdot)$, as described in (4.9). Incorporating this expression, (A.1) can be reformulated as

$$\bar{P}_b = \int_V \frac{g(h_{1,R}, h_{1,I}, h_{2,R}, h_{2,I}) z(h_{1,R}, h_{1,I}, h_{2,R}, h_{2,I})}{z(h_{1,R}, h_{1,I}, h_{2,R}, h_{2,I})} d\hat{h} \tag{A.3}$$

Afterwards, we generate J random points for all integral variables from corresponding sampling functions as $\{\mathbf{h}^{(1)}, \mathbf{h}^{(2)}, \ldots, \mathbf{h}^{(J)}\}$ where $\mathbf{h}^{(j)} = [h_{1,R}^{(j)}, h_{1,I}^{(j)}, h_{2,R}^{(j)}, h_{2,I}^{(j)}]$ for $j = 1, 2, \ldots, J$. Then the importance weights are calculated as follows

$$w(\mathbf{h}^{(j)}) = \frac{g(h_{1,R}^{(j)}, h_{1,I}^{(j)}, h_{2,R}^{(j)}, h_{2,I}^{(j)}) z(h_{1,R}^{(j)}, h_{1,I}^{(j)}, h_{2,R}^{(j)}, h_{2,I}^{(j)})}{z(h_{1,R}^{(j)}, h_{1,I}^{(j)}, h_{2,R}^{(j)}, h_{2,I}^{(j)})}. \tag{A.4}$$

The integral is estimated using the average of these weights as expressed below: [Yuan et al., 2020]

$$\bar{P}_b = \frac{1}{J}\sum_{j=1}^{J} w(\mathbf{h}^{(j)}). \tag{A.5}$$

For unconditional BEP curves, $J = 10^6$ random sample points are used for all integral estimations.

A.2 Monte Carlo Integration Method for the ND-NOMA for three users system

Monte Carlo integration is a widely utilized technique for estimating integrals that are difficult or impossible to compute analytically, especially in high-dimensional problems [Yapici et al., 2024]. In the context of the ND-NOMA for three users system, the unconditional BEP can be expressed as the following multidimensional integral:

$$\bar{P}_b = \int_V g(h_{1,R}, h_{1,I}, h_{2,R}, h_{2,I}, h_{3,R}, h_{3,I})\, d\hat{h}, \tag{A.6}$$

where the function $g(\cdot)$ is defined as:

$$g = P_b \cdot f(h_{1,R})f(h_{1,I})f(h_{2,R})f(h_{2,I})f(h_{3,R})f(h_{3,I}), \tag{A.7}$$

and the integration differential is denoted by $d\hat{h} = dh_{1,R}dh_{1,I}dh_{2,R}dh_{2,I}dh_{3,R}dh_{3,I}$. Here, $f(\cdot)$ represents the marginal probability density functions of the Rician distributed channel coefficients. The integration region V spans the entire range of possible channel realizations.

To enhance computational efficiency, we employ importance sampling by introducing a joint sampling distribution that factorizes across all variables:

$$z(\cdot) = \prod_{i=1}^{3} z(h_{i,R})z(h_{i,I}), \tag{A.8}$$

where $z(\cdot)$ is selected to closely match the actual distributions of the fading variables.

The integral is then estimated using a Monte Carlo approximation based on J independently drawn samples $\mathbf{h}^{(j)} = [h_{1,R}^{(j)}, h_{1,I}^{(j)}, h_{2,R}^{(j)}, h_{2,I}^{(j)}, h_{3,R}^{(j)}, h_{3,I}^{(j)}]$. The estimate becomes:

$$\bar{P}_b \approx \frac{1}{J} \sum_{j=1}^{J} \frac{g(\mathbf{h}^{(j)})}{z(\mathbf{h}^{(j)})}. \tag{A.9}$$

In our simulations, we set $J = 10^6$ sample points to ensure high-accuracy estimates for the BEP under various Rician fading conditions in the ND-NOMA for three users system.